



University of
Stavanger

Faculty of Science and Technology

MASTER'S THESIS

Study program: Master in Industrial Economics	Spring semester, 2012.
Specialization: Reservoir Engineering	Open
Writer: Silje Storås (Writer's signature)
Faculty supervisor: Professor Tor Austad	
Supervisors: Skule Strand and Tina Puntervold	
Title of thesis: Low Salinity EOR-potential for Yme at Reservoir Conditions - An Experimental Study	
Credits (ECTS): 30	
Key words: <ul style="list-style-type: none">- Enhanced Oil Recovery- Low Salinity Waterflooding- Sandstone- Wettability- Local pH change- CaSO₄ – effect	Pages: 79 + enclosure: 8 Stavanger, 15/06-2012.

Acknowledgements

I am grateful for all the help, support and guidance I have got carrying out this thesis. There are many people who have contributed in different ways and I would like to thank every one of you.

First, I would like to thank Professor Tor Austad at the University of Stavanger, for providing me with such an exciting and challenging master thesis.

A specially thank goes to both of my supervisors, Associate Professor Skule Strand and Post Doctor Tina Puntervold, for sharing their experience and knowledge, and providing me with literature. I also appreciate Strand for answering all of my questions, and Puntervold for very good proofreading of my thesis.

I wish to thank Laboratory Assistant Hakan Aksulu for all the help and guidance during the experimental work at the laboratory.

Finally, I would like to thank my co-worker at the laboratory Master Student, Kine Navratil, for a good collaboration during the experimental work on both of our thesis, and providing me with results from her work.

Silje Storås

Abstract

The composition of the water injected into a reservoir affects the oil recovery. Injecting water with low salinity (LowSal) has been proved by several studies to improve the water wetness of the rock and thereby increase the recovered oil in sandstone reservoirs. The mechanism behind the LowSal enhanced oil recovery (EOR) process has been discussed the last decade, but none of the suggested mechanisms has been accepted as the main one contributing for the observed LowSal EOR effect.

The decrease in salinity is not the main reason for the wettability alteration in a LowSal process. Previous work have concluded that adsorption and desorption of polar material onto clay are mainly pH dependent. In this experimental study, a sandstone reservoir core was waterflooded with sequence, FW-SW-d₅₀SW-LowSal Al, at reservoir temperature 110°C. Both pH and the concentration of Ca²⁺ and SO₄²⁻ of the effluent were recorded during the flooding. When switching from FW to SW and d₅₀SW an increase in pH was observed, while switching to LowSal Al the pH decreased to the initial value of the injected brine. When the pH increased, the organic material which was initially adsorbed onto the clay, desorbed. The pH gradient, ΔpH, was linked to the concentration of Ca²⁺, salinity of the brine, temperature and the presence of anhydrite, CaSO₄, in the rock material. A higher concentration of Ca²⁺ caused less adsorption, and a wetting alteration towards a more water-wet system. The high temperature caused both the ΔpH and desorption of Ca²⁺ to decrease because the ions have increasing affinity towards the clay surface. Not having CaSO₄ present in the core, a higher ΔpH and desorption of Ca²⁺ was observed, compared to rock material containing CaSO₄.

Table of content

Acknowledgements	2
Abstract	4
Table of content.....	6
1 Introduction	8
2 Work Objectives.....	10
3 Theory	12
3.1 Recovery stages.....	12
3.1.1 Primary recovery	12
3.1.2 Secondary recovery	12
3.1.3 Tertiary recovery/EOR.....	13
3.2 Yme Field.....	14
3.3 Sandstones.....	16
3.3.1 Clay minerals.....	16
3.3.2 Anhydrite.....	20
3.4 Wettability.....	21
3.5 Displacement forces	25
3.5.1 Capillary Forces.....	25
3.5.2 Viscous Forces	26
3.5.3 Gravity Forces	27
3.6 Low salinity waterflooding.....	29
3.6.1 Requirements.....	29
3.6.1.1 Rock.....	30
3.6.1.2 Oil.....	30
3.6.1.3 Brine	31
3.6.1.4 LowSal injection fluid	31
3.6.1.5 Produced water	31
3.6.1.6 Temperature.....	31
3.6.2 Mechanisms.....	32
4 Experimental work	42
4.1 Materials.....	42
4.1.1 Rock.....	42
4.1.2 Oil.....	44
4.1.3 Brines.....	44

4.2	Experimental procedures	47
4.2.1	Measurement of acid and base numbers.....	47
4.2.2	Core cleaning.....	47
4.2.2.1	Removing CaSO ₄	48
4.2.3	Density measurement	49
4.2.3.1	Density of Yme FW and d ₅ Yme FW.....	49
4.2.4	Water saturation.....	50
4.2.5	Pore volume measurement	51
4.2.6	Porosity measurement	51
4.2.7	Initial water saturation.....	52
4.2.8	Asphaltene content	53
4.2.9	Oil saturation	53
4.2.10	Aging of the core.....	53
4.2.11	Waterflooding – main test	54
4.2.11.1	Density and pH measurements of effluent water.....	55
4.2.11.2	Oil recovery calculation	56
4.2.11.3	Volume correction: Shrinkage factor	56
4.2.11.4	Cation and anion content	58
4.2.12	Uncertainties in the experimental work.....	59
5	Results	60
5.1	Yme Core#22	60
5.2	Yme Core#23	62
6	Discussion	66
7	Conclusions	70
8	Abbreviations	72
9	References	74
	Appendices	80
	Appendix 1: Composition of the rock	80
	Appendix 2: Compositions of Brines	81
	Appendix 3: Main test data	85
	Appendix 4: Cation and Anion Content	85

1 Introduction

For several years there has been great interest of finding out how to displace the remaining oil in a producing reservoir. Studies during these years have proven that enhanced oil recovery (EOR) in sandstone reservoirs can be obtained by waterflooding, where the injected water has a composition different from the formation water (FW). This “smart water” is simply made by modifying the ion composition of the water, and results in improved wetting properties of the reservoir causing an optimized oil recovery during production.

Looking at the big picture, the overall goal by injecting smart water into a porous reservoir is to displace remaining oil, increase the oil recovery, which at the end will provide more money for the oil companies, improving the countries welfare, as illustrated in Figure 1-1.

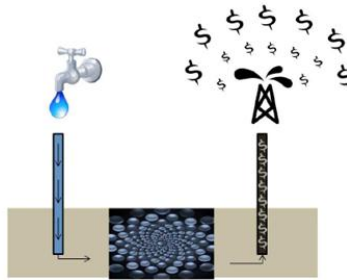


Figure 1-1: Illustration of the overall smart-water effect (Strand et al., 2012).

The estimated remaining oil reserves left on the Yme field is 12 mill. Sm³. The sandstone reservoir has already been flooded with sea water (SW), and the experimental study of this thesis has the purpose to look at the EOR potential of the field. Water with low salinity (LowSal) is injected into a sandstone reservoir core from Yme, hoping that more oil will be produced. The overall goal of this master thesis is therefore to observe LowSal effect and contribute with useful information to further research on the LowSal mechanism.

It has been shown that the brine, crude oil and rock all play an important role in the oil recovery process. However, these interactions are complex and not easy to understand. Several mechanisms, both physical and chemical, behind the LowSal EOR process have been proposed the last decade, but none of them has so far been generally accepted as the main one responsible for the observed LowSal effect. In order to observe any effect, researchers have however agreed upon some general conditions that must be fulfilled:

- The rock must contain active clay, and have initial water saturation.
- The oil must be a crude oil containing polar components.
- The LowSal water injected must have salinity below 40 000 ppm.

This master thesis starts by introducing some general theory. Oil recovery stages are defined, information on the Yme field is presented, and characteristics of sandstones are described. Further, mechanisms of displacing oil are reviewed before specifying the LowSal topic. Both former and newer suggestions of the LowSal effect are proposed. The experimental part of the thesis contains all the materials, procedures and apparatus used during the experimental study. The results are listed and discussed. Finally, all the main results are summed up in the conclusion. In the appendices at the end of the thesis, some additional detailed data which may be of interest are listed.

2 Work Objectives

In this thesis, the main objective of the experimental work is to evaluate the enhanced oil recovery (EOR) potential for a sandstone reservoir, by low salinity (LowSal) waterflooding.

The effect of temperature, pH and Ca^{2+} concentration, related to wettability alteration of the system, was observed and evaluated.

Further, an evaluation of the presence of anhydrite, CaSO_4 , in the rock was performed.

A flooding test was conducted at reservoir conditions on a sandstone reservoir core not containing any CaSO_4 . The results were compared with results from a similar study where a CaSO_4 was present in the rock material, done by Master Student, Kine Navratil.

The study in this thesis will contribute with useful information to further research on the LowSal mechanism in the future.

3 Theory

3.1 Recovery stages

A reservoir begins to produce when oil moves from the reservoir to the well. The production processes which moves the oil can be divided into three stages of recovery:

1. Primary recovery
2. Secondary recovery
3. Tertiary recovery/Enhanced oil recovery (EOR)

These stages are described in the following subsections.

3.1.1 Primary recovery

The first stage of production is primary oil recovery. In this stage, hydrocarbons (HC) are displaced from the reservoir to the well and up to the surface by natural energy present in the reservoir. Sources of natural energy are solution-gas drive, gas-cap drive, natural water drive, fluid and rock expansion, and gravity drainage (Green & Willhite, 1998). The high natural differential pressure between the reservoir and the inside of the well causes the movement of HC towards the well. Due to pressure depletion during production, it is necessary to implement artificial lift to increase the differential pressure and keep up the reservoir production (Ahmed, 2001). Primary recovery is a relatively inefficient process where only 10-30 % of the initial HC in place are produced (Green & Willhite, 1998).

3.1.2 Secondary recovery

The second stage of HC production is secondary oil recovery. In this stage, supplemental energy is provided to accelerate and increase the oil recovery when primary recovery has reached its limit of production. External sources such as water injection or gas injection are used to maintain the pressure or to improve sweep efficiency so that residual oil is displaced toward producing wells (Green & Willhite, 1998). Today, waterflooding is perhaps the most common method (Ahmed, 2001; Green & Willhite, 1998). Secondary recovery produces 30-50 % of the original oil in place (OOIP).

3.1.3 Tertiary recovery/EOR

The third stage of HC production is tertiary recovery, also known as EOR. After both primary and secondary oil recovery becomes uneconomical, oil left in the reservoir can be displaced by injection of gases or liquid chemicals, or by use of thermal energy. These EOR methods supplement the natural energy present in the reservoir to displace oil and interact with the reservoir rock or oil system to enhance the movement of oil through the formation (Green & Willhite, 1998; Ahmed, 2001; Fanchi, 2010). Another common concept is improved oil recovery (IOR), which includes EOR and reservoir characterization, improved reservoir management, and infill drilling. As mentioned in the previous section, waterflooding is a common method of secondary recovery. Several studies over the past decade have proven that by injecting water, the oil recovery is increased due to a wettability modification towards a more water-wet condition. Combined with the fact that the composition of the injected water is different from the formation water (FW), this may characterize waterflooding as an EOR process (Green & Willhite, 1998).

3.2 Yme Field

The Yme field is located in the southeastern part of the North Sea, as shown in Figure 3-1, 77-93 meters beneath the surface of the sea. Yme was discovered in 1987 and the production started in 1996. Statoil operated the field and produced until 2001, then the operation was considered unprofitable and the field was shut down. Later, Talisman Energy became the operator and decided in 2006 to recover the remaining resources with a new jack-up production facility, showed in Figure 3-2. This made Yme the first oil field on the Norwegian continental shelf to be redeveloped after being shut down. When the production will start again, is currently not known (Oljedirektoratet, 2011).

The Norwegian Petroleum Department estimates that the remaining oil reserves per 31.12.2011, were 12 million Sm³ (The NPD's Fact-pages, 2012).

The reservoir is located at a depth of 3 150 meters in Middle Jurassic sandstones in the Sandnes Formation. It contains two separate main structures, Gamma and Beta, which comprises five deposits. The Beta structure is being developed with subsea wells, while the new facility is located on the sea bed above the Gamma structure. Yme will mainly be produced by water injection (Oljedirektoratet, 2011).

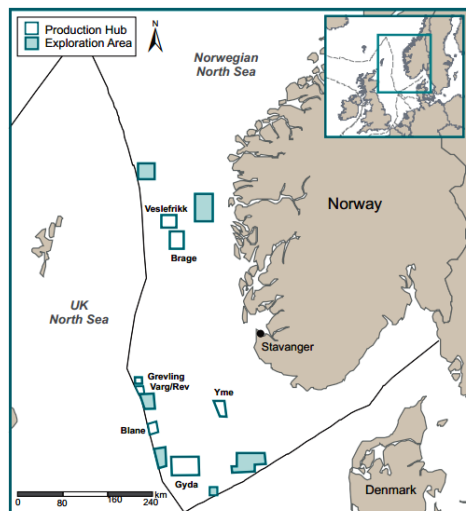


Figure 3-1: Location of the Yme field (Annual Information Form of Talisman Energy Inc., 2011).



Figure 3-2: Jack-up facility on the Yme field (The NPD's Fact-pages, 2012).

In 1997, the deviated well 9/2-7 S was drilled as an exploration well to identify the oil potential of the Beta Vest structure with the Sandnes Formation sandstones as the target horizon (The NPD's Fact-pages, 2012). Two cores were cut from this formation in this well, in the interval 3868 - 3923 m. A small core plug from one of these cores was used in the experimental work of this thesis. Well 9/2-7 S was reclassified to development well 9/2-B-3H in 1999, and used for injection (The NPD's Fact-pages, 2012).

3.3 Sandstones

One of the main reservoir rocks in the world is sandstone. Sandstone reservoirs account for 80 % of all reservoirs and 60 % of oil reserves (Cossé, 1998). Sandstone is a sedimentary rock formed at the Earth's surface by deposition of clastic sediments or chemical precipitates, followed by compaction and cementation (Aadnøy & Looyeh, 2011). The rock is predominantly composed of quartz, feldspar and rock fragments. The rock grains are sand-sized and bonded together with cements like silica, calcium carbonate, iron oxide and clay minerals. Sandstone has a density of 2.65 g/cm^3 and what makes them good reservoir rocks is their relatively high porosity, typical 7-20%, and high permeability (Zolotukhin & Ursin, 2000).

3.3.1 Clay minerals

Surface area, chemical composition and temperature will characterize the reactivity of a mineral. Due to the greater specific surface area compared with other minerals, clays are probably the most reactive component during well-stimulation operations. Clays may form in the pores and are mainly composed of silicon, aluminum and water (Schlumberger Oilfield Glossary, 2012).

Sandstone reservoir clays typically have a crystal structure consisting of tetrahedral silica and octahedral aluminum layers. The octahedral layer is made up of aluminum or magnesium atoms, bonded together by oxygen atoms (Darley & Gray, 1988), see Figure 3-3.

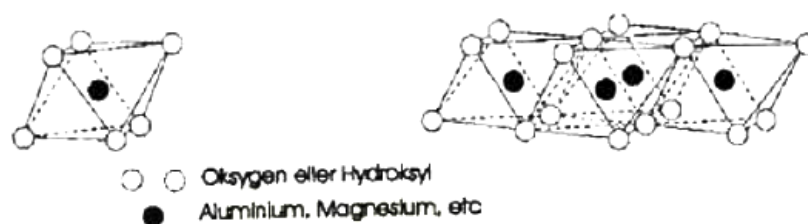


Figure 3-3: The octahedral sheet (IDF, 1982).

A tetrahedral layer consists of silicon atoms which are coordinated with four oxygen atoms each. It forms a hexagonal network of oxygen atoms (Darley & Gray, 1988), see Figure 3-4.

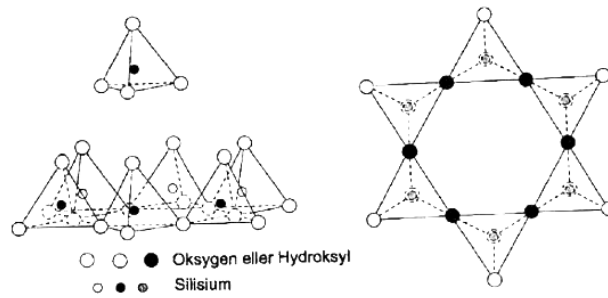


Figure 3-4: Structure of the tetrahedral layer (IDF, 1982).

The octahedral and tetrahedral layers are bonded together by sharing common oxygen atoms as shown in Figure 3-5.

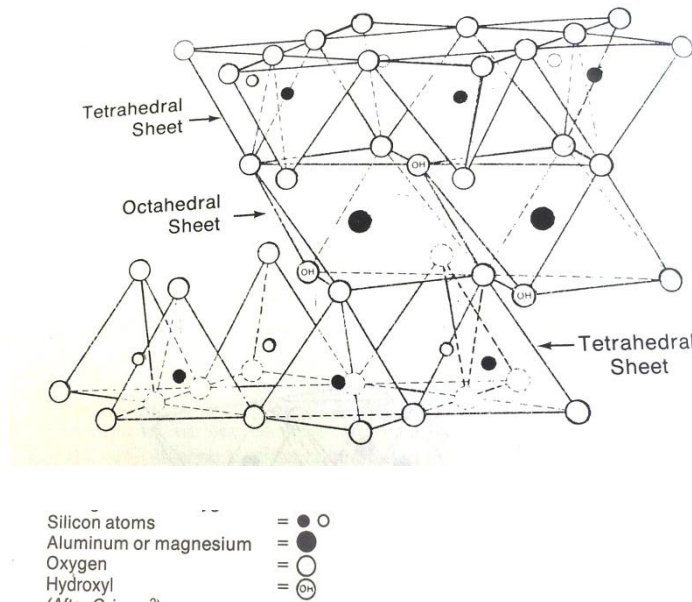


Figure 3-5: Bonding between one octahedral sheet and two tetrahedral sheets through shared oxygen atoms (Darley & Gray, 1988).

Due to a structural imbalance in the silica or in the aluminum layer and also at the edge surfaces that causes a negative charge on the clay surface, the clay minerals are able to exchange cations adsorbed between their layers and to their external surfaces. This characteristic makes the clay a cation exchange material (Austad et al., 2010; Morad & Worden, 2003).

Cation exchange will occur when one or more injected fluids differ in electrolyte composition from the initial fluid saturating the rock (Bavière, 1991). The different ions have different affinities for clays. The order of affinity for the different ions are as followed (RezaeiDoust et al., 2011):



The combination of the octahedral and tetrahedral layers, characterizes the different types of clay. In reservoir sandstone the most common minerals are kaolinite, illite/mica, chlorite and smectites.

Kaolinite has a 1:1 structure which means it is a two-layered clay. It is composed by one tetrahedral silica sheet and one octahedral aluminum sheet tied together strongly by hydrogen, as illustrated in Figure 3-6. This strong bonding together with a small surface area also means that the cation exchange capacity (CEC) is low. Transformation of the kaolinite to illite or chlorite may occur at greater depths (Darley & Gray, 1988; Austad et al., 2010).

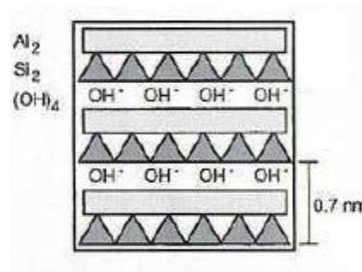


Figure 3-6: Illustration of kaolinite. Triangular shapes represent the tetrahedral layers and the rectangular shapes represent the octahedral layers (Morad & Worden, 2003).

Illite/mica has a 2:1 structure where one octahedral aluminum layer lies between two tetrahedral silica layers as illustrated in Figure 3-7. The substitution occurs in the tetrahedral silica layer where silicon (Si^{4+}) is replaced by aluminum (Al^{3+}) which creates a negatively charged surface. Both the surface area and the CEC are larger than for kaolinite (Darley & Gray, 1988; Austad et al., 2010).

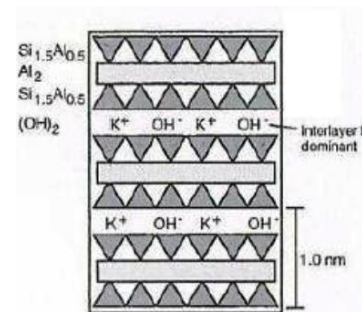


Figure 3-7: Illustration of illite. Triangular shapes represent the tetrahedral layers and the rectangular shape represents the octahedral layers (Morad & Worden, 2003).

Smectites also have a 2:1 structure and a composition similar to illite and mica, illustrated in Figure 3-8. Montmorillonite is a well-known smectite clay mineral which tends to swell when exposed to water. In montmorillonite the substitution occurs in the octahedral aluminum layer where aluminum (Al^{3+}) gets replaced by magnesium (Mg^{2+}) or iron (Fe^{3+}). Compared to the other clay minerals, montmorillonite has the highest CEC due to their swelling property which makes it easier to exchange the cations (Darley & Gray, 1988; Austad et al., 2010).

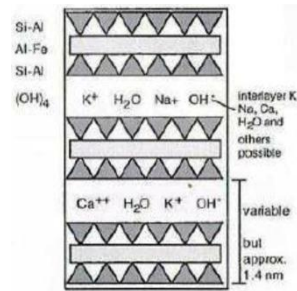


Figure 3-8: Illustration of montmorillonite. Triangular shapes represent the tetrahedral layers and the rectangular shape represents the octahedral layers (Morad & Worden, 2003).

Chlorite has a 2:1:1 structure where mica with structure 2:1 is bonded with a brucite layer, illustrated in Figure 3-9. The substitution occurs in the octahedral aluminum layer where aluminum (Al^{3+}) is replaced by silicon (Si^{4+}) creating a positive charge. CEC is the same as for illite and mica, but the surface area is the largest of the clay minerals (Darley & Gray, 1988; Austad et al., 2010).

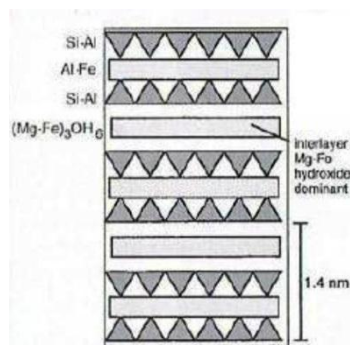


Figure 3-9: Illustration of chlorite. Triangular shapes represent the tetrahedral layers and the rectangular shape represents the octahedral layers (Morad & Worden, 2003).

Some of the properties of the clay minerals discussed above are listed in Table 3-1.

Table 3-1: Properties of common clay minerals (IDF, 1982).

Property	Kaolinite	Illite/Mica	Montmorillonite	Chlorite
Layers	1:1	2:1	2:1	2:1:1
Particle size [micron]	5-0.5	Large sheets to 0.5	2-0.1	5-0.1
Cation exchange capacity [meq/100g]	3-15	10-40	80-150	10-40
Surface area BET-N ₂ [m ² /g]	15-25	50-110	30-80	140

3.3.2 Anhydrite

Anhydrite is a member of the evaporate mineral group. The colorless or greyish-white mineral, can be found in sedimentary rocks. It is formed by evaporation of seawater or by dehydration of gypsum, which is another sulphate mineral, found in evaporates. It is composed of anhydrous calcium sulphate and has the formula CaSO₄. When exposed to water, anhydrite transforms to gypsum (CaSO₄×2H₂O) by the absorption of water (Schlumberger Oilfield Glossary, 2012).

3.4 Wettability

Wettability is a property that can be defined as the tendency of one fluid to spread on or adhere to a solid surface in the presence of other immiscible fluids (Ahmed, 2001).

Reservoir wettability determines the flow of oil and water in the reservoir. The wetting condition in a rock-fluid system depends on the interfacial tension (IFT), which refers to the tension between liquids at a liquid-liquid interface. IFT depends on the composition of the two fluids at the interface between phases (Fanchi, 2010).

Wettability is measured by the contact angle where two immiscible fluids interface meets the solid surface, as illustrated in Figure 3-10. Different wetting conditions and their respective angle of contact are listed in Table 3-2. The angle is measured through the denser phase with Equation 2 (Dandekar, 2006).

$$\sigma_{SO} - \sigma_{SW} = \sigma_{OW} \cos\theta \quad (2)$$

Where:

σ_{SO} = Interfacial tension between oil and solid [dynes/cm]

σ_{SW} = Interfacial tension between water and solid [dynes/cm]

σ_{OW} = Interfacial tension between oil and water [dynes/cm]

θ = Contact angle at oil-water-solid interface measured through the water phase [degrees]

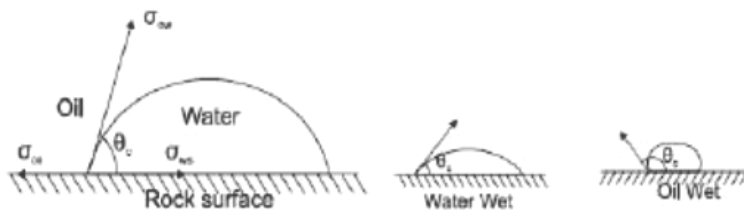


Figure 3-10: Illustration of the contact angle θ , through the water phase (Strand, 2005).

Table 3-2: Wetting conditions for a water-oil system (Fanchi, 2010).

Wetting Condition	Contact Angle [degrees]
Strongly water-wet	0-30
Moderately water-wet	30-75
Neutrally wet	75-105
Moderately oil-wet	105-150
Strongly oil-wet	150-180

The contact angle indicates the wettability condition in a reservoir. The five wetting conditions are illustrated in Figure 3-11 below.

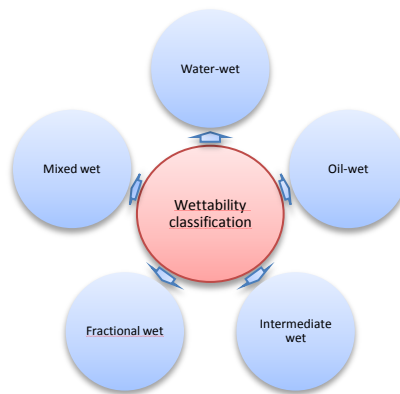


Figure 3-11: Illustration of the five wettability categories.

Water-wet

In a water-wet rock, the surface prefers the water phase rather than the oil. For a completely water-wet rock, the oil is centered in the pores as droplets surrounded by water, not covering any of the rock surfaces, as illustrated in Figure 3-12. The potential for increased oil recovery through continued waterflooding is low for these systems. A completely water-wet system has an angle of contact of 0° (Dandekar, 2006).

Oil-wet

An oil-wet rock is exactly the opposite of a water-wet rock. The oil exists like a film on the surface of the rock, and the water is centered in the pores as droplets, as illustrated in Figure 3-12. A completely oil-wet system has a contact angle of 180° (Dandekar, 2006).

Fractional wet

Fractional wettability refers to a state where some of the pores are water-wet, while others are oil-wet. The different minerals in the rock have different chemical properties leading to variations in preferential wetting of water and oil throughout the rock surface (Dandekar, 2006).

Mixed wet

Mixed wettability is a special type of fractional wettability. In some parts the water occupies the smaller pores and are water-wet containing no oil, while other parts the oil fill up larger pores forming continuous paths, resulting in an oil-wet surface (Dandekar, 2006).

Intermediate wet

Intermediate wet refers to a state where the rock surface prefers both the oil and water phases. This is a state that includes the sub-classes of both fractional and mixed wettability. The state where the rock surface has an equal preference of oil and water is called neutral wettability. The contact angle in this case is 90° (Dandekar, 2006).

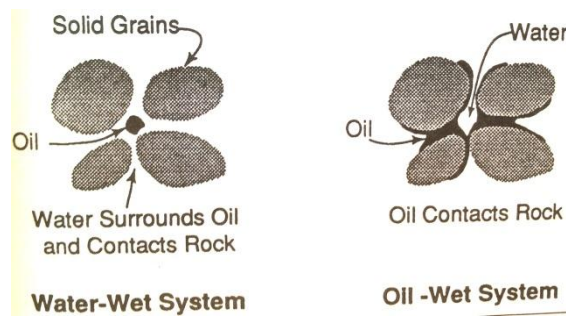


Figure 3-12: Illustration of a water-wet and an oil-wet system (Green & Willhite, 1998).

The wettability alteration of a reservoir can be done by changing the parameters that influence the wettability. Some of the parameters which influence the wettability during a waterflooding are illustrated in Figure 3-13.

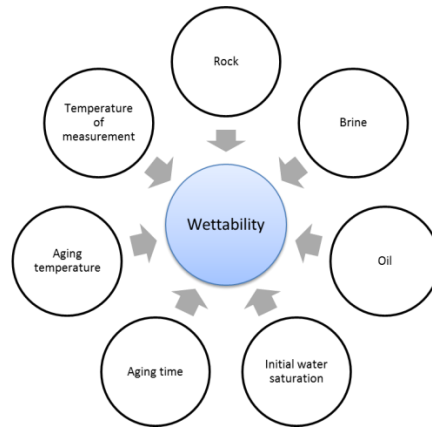


Figure 3-13: Parameters that influences the wettability during waterflooding.

Several reports of experimental work on wettability conditions have been published. Jadhunandan and Morrow (1995) found the optimum wetting condition for oil recovery by waterflooding to be weakly water-wet. A decreasing water-wetness increases the oil recovery, and an increasing oil-wetness decreases the oil recovery.

3.5 Displacement forces

The main displacement forces which act on oil, gas and water inside a pore system are capillary forces, gravity forces and viscous forces.

3.5.1 Capillary Forces

Capillary pressure can be defined as the pressure difference across a curved interface between two immiscible fluids, or as the pressure difference across the interface between a non-wetting and a wetting phase (Green & Willhite, 1998). This can be illustrated, as in Figure 3-14, by fluid rise in a capillary tube.

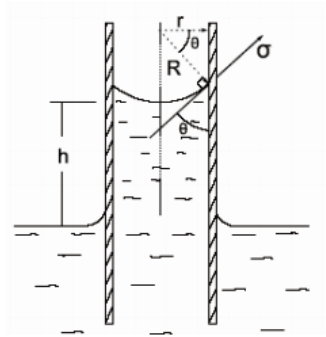


Figure 3-14: Fluid rise in a capillary tube used for measuring capillary pressure (Strand, 2005).

Capillary pressure is expressed by the Laplace equation, Equation 3 (Archer & Wall, 1999).

$$P_C = P_O - P_W = \sigma \left(\frac{1}{R_1} + \frac{1}{R_2} \right) = \frac{2\sigma_{OW} \cos \theta}{r} \quad (3)$$

Where:

P_C = Capillary pressure [dynes/cm²]

P_O = Pressure in the oil phase [dynes/cm²]

P_W = Pressure in the water phase [dynes/cm²]

σ_{OW} = Interfacial tension between oil and water [dynes/cm]

R_1, R_2 = The curvature radii of interface between oil and water [cm]

θ = Contact angle measured through the water phase [degrees]

r = Radius of the pore [cm]

The equation indicates that the capillary pressure is related to the fluid (by IFT), the relative wetting of the fluids (through θ), and the size of the capillary (r). Whether the capillary pressure is positive or negative depends on which phase the pressure is lower (Green & Willhite, 1998). A negative capillary pressure indicates that the oil is the wetting phase, and positive value indicates that it is water that is the wetting phase. In reservoirs, it is most common that water is the wetting phase and oil is the non-wetting phase.

3.5.2 Viscous Forces

In a porous medium, viscous forces are reflected in the magnitude of the pressure drop that occurs as a result of a flow of a fluid through the medium. For simplicity, the porous medium can be considered as a bundle of parallel capillary tubes. The pressure drop for laminar flow through a single tube is then expressed by Equation 4 (Green & Willhite, 1998).

$$\Delta p = -\frac{8\mu L v_{avg}}{r^2 g_c} \quad (4)$$

Where:

Δp = Pressure drop across the capillary tube, p_2-p_1 [lbf/ft²]

L = Capillary tube length [ft]

r = Capillary tube radius [ft]

v_{avg} = Average velocity in the capillary tube [ft /sec]

μ = Viscosity of flowing fluid [lbm/ (ft-sec)]

g_c = Conversion factor

Viscous forces force the fluid through the reservoir core by overcoming the capillary barrier in the pores. The relationship between the viscous and capillary force is usually expressed by the dimensionless capillary number, N_{ca} , Equation 5 (Bavière, 1991).

$$N_{ca} = \frac{F_V}{F_C} = \frac{v\mu_W}{\sigma_{OW}} \quad (5)$$

Where:

N_{ca} = Capillary number

F_V = Viscous force [dynes]

F_C = Capillary force [dynes]

v = Interstitial pore velocity [ft/hr]

μ_W = Viscosity of the water [cp]

σ_{OW} = Interfacial tension (IFT) between the displaced and displacing phases [dynes/cm²]

Where the capillary numbers are less than 10^{-6} , the residual oil is relatively constant (Green & Willhite, 1998). For typical waterflood conditions the capillary number is less than 10^{-6} (Bavière, 1991). Most common are capillary numbers on the order of 10^{-7} . Increasing the N_{ca} to more than about 10^{-5} in a flood will decrease the magnitude of residual oil, and by increasing it to values on the order of 10^{-2} , virtually all oil is recovered. Different experiments have verified that the N_{ca} can be increased by increasing the flow rate of the displacing fluid, increasing the viscosity of the displacing fluid, or reducing IFT between the displaced and displacing fluids (Green & Willhite, 1998).

3.5.3 Gravity Forces

When there is a large difference in the densities between the injected and the displaced fluids in a reservoir, the gravity forces are important (Green & Willhite, 1998). Because of the buoyancy forces, the lighter fluid in the mixture of immiscible fluids will be displaced upwards. The pressure difference is expressed by Equation 6.

$$\Delta P_g = \Delta \rho g h \quad (6)$$

Where:

ΔP_g = Pressure difference between oil and water [Pa]

$\Delta \rho$ = Density difference between oil and water [kg/m³]

g = Gravity acceleration [m/s²]

h = Height of the liquid column [m]

How much the gravity forces will influence the fluid movement in the reservoir, is controlled by the density difference between the fluid phases, the height of liquid column, the magnitude of capillary forces related to IFT, wettability and permeability (Strand, 2005).

3.6 Low salinity waterflooding

Waterflooding is a physical process where water is injected into a reservoir to displace residual oil. For a very long time this process was considered a technique for pressure maintenance, pushing the oil out of the reservoir, but recent experimental work and studies has suggested that the composition of the brine is crucial; “water is not just water!”

By injecting water with a modified ion composition, called “smart water”, the wetting properties will change towards a more water-wet reservoir in both sandstones and carbonates. This will result in an optimization of the fluid flow and increase the oil recovery.

Experimental work performed by injecting water with LowSal during waterflooding, has indicated an increased oil recovery. Lager et al. (2008a) states that by injecting LowSal water with the right composition to the right reservoir, it is possible to reach an increased recovery of up to 40%.

The recovery process is influenced by the interactions between the crude oil, brine and rock. These interactions are very complex and not easy to understand. Several mechanisms, both physical and chemical, behind the LowSal EOR process have been proposed the last decade, but none of them has so far been generally accepted as the main one responsible for the observed LowSal effect.

In the next subsections, conditions for obtaining a LowSal effect and some of the different mechanisms proposed over the last years are being presented.

3.6.1 Requirements

To obtain LowSal effects there are some required conditions to have in mind. The main conditions listed in Figure 3-15 and described in the following subsections, are taken from RezaeiDoust et al. (2009) and Austad et al. (2010).

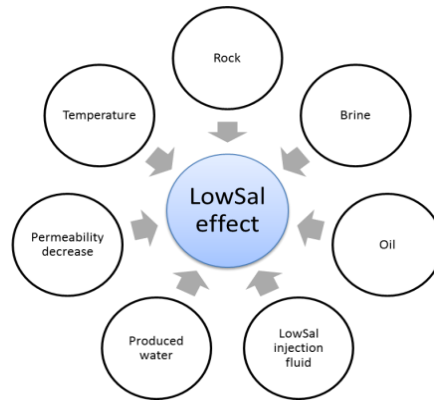


Figure 3-15: Main parameters for observing a LowSal effect.

3.6.1.1 Rock

It is crucial that we have a porous medium such as sandstone. LowSal effects have not been documented in pure carbonates. Although recent study shows that we are almost getting there with carbonates too, the mechanisms differ from those in sandstone. On the other hand, LowSal effects have been observed in sandstone containing dolomite crystals (Pu et al., 2008). Most important is the presence of clay in the sandstone, and type of clay may also play a role. The surface charges, bonds and cation exchange will all affect the recovery when injecting LowSal water.

3.6.1.2 Oil

The oil must contain polar components which are naturally occurring surface-active agents, like acids and bases, which can change the wettability away from water-wet (Jerauld et al., 2008). No effect has been observed by use of oil free from polar components.

The acid number (AN) is defined as the amount of potassium hydroxide (KOH) in milligrams, required for neutralizing 1 g of the petroleum acid in the crude oil, and reversely, the base number (BN) is defined as the amount of KOH in milligrams, required neutralizing 1 g of the petroleum base (Green & Willhite, 1998).

When water is present, the oil and rock surfaces become charged. Their polar components behave as acids and bases by giving up a proton and becoming negatively charged, and gaining a proton and becoming positively charged, respectively (Buckley and Liu, 1998). These surface charges influence the adsorption behavior and thus wettability during injection of LowSal water.

3.6.1.3 Brine

The FW must contain divalent cations, like Ca^{2+} and Mg^{2+} , which can interact with the oil and the surface rock and create bonds (Lager et al., 2008b). Tang (1998) concludes that the salinity and pH of the brine affect the surface charge of the rock and oil/brine interfaces which affect the adsorption of polar components and therefore the wettability.

Initial FW must be present and the efficiency is related to initial water saturation, S_{wi} . Tang and Morrow (1999) propose that when a core is initially 100% saturated with crude oil, $S_{wi} = 0$, then the oil recovery will not be affected by changes in salinity of the injected brine by waterflooding.

3.6.1.4 LowSal injection fluid

The general belief is that the LowSal injection fluid must have a salinity ranging from 1000-2000 ppm, but LowSal effects have been observed up to 40 000 ppm in recent work done by RazeiDoust (2011). The fluid also appears to be sensitive to ionic composition (Ca^{2+} vs. Na^+), affecting the interactions between the injected and initial water, the rock mineral composition and the crude oil, resulting in possible wettability alteration.

3.6.1.5 Produced water

The produced water is used for pH measurements. For a non-buffered system, the pH of the effluent water usually increases about 1-3 pH units when injecting the LowSal fluid. It has not been verified that an increase in pH is needed to observe LowSal effects. In some cases, production of fines has been detected, but LowSal effects have also been observed without visible production of fines (Lager et al., 2008b).

3.6.1.6 Temperature

When considering temperature, there seems to be no limitations to where LowSal effects can be observed. However, most of the reported studies have been performed at temperatures below 100°C. Recent LowSal work indicates that an effect may be difficult at high temperatures. Tang (1998) proposes that by increasing the aging time and temperature, changes the wetting from strongly water-wet towards oil-wet.

3.6.2 Mechanisms

Probably, the LowSal effect is a result of different mechanisms acting together, each with its own contribution. Some of the different mechanisms, which have been proposed up to now, are:

Migration of fines

The migration of fines theory was suggested by Tang and Morrow (1999). In the paper they state that LowSal water will release fines, which are small clay particles. Some crude oil will adhere to the fine particles as droplets and when injecting LowSal water some of the oil will be produced together with these fines as shown in Figure 3-16. A wettability alteration occurs, making the clay more water-wet. The released fines will also improve the sweep efficiency. Fines will slowly block the pores throats which lead to a pressure buildup forcing the water to flow into the non-swept pores with residual oil and consequently improve the sweep efficiency (Skauge et al., 2008). However, LowSal effects without production of fines have been observed in later work.

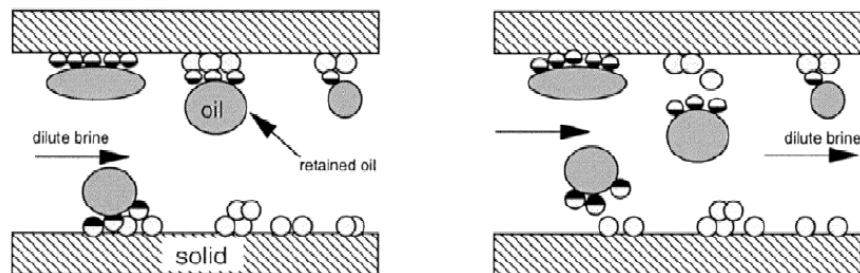
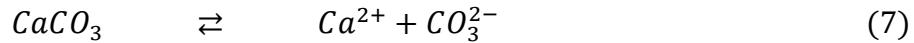


Figure 3-16: Illustration to the left shows the oil before LowSal waterflooding and the illustration to the right shows the oil which detaches to the fines during LowSal waterflooding (Tang & Morrow, 1999).

Increase in pH

McGuire et al. (2005) suggests in their paper that the observed increase in oil recovery by injection of LowSal brine was similar to alkaline flooding. Furthermore, they state that the increase in pH, normally 1-3 pH units, after LowSal waterflooding is due to generation of surfactants from the residual oil. This generation requires that the crude oil has an AN greater than 0.2 mg KOH/g (RezaeiDoust et al., 2009). LowSal effects have however been observed with lower AN, which also makes this mechanism doubtful. Reduction in reservoir oil/water IFT and changes in wettability may also occur with elevated pH, increasing oil recovery.

Two mechanisms, carbonate dissolution and cation exchange, can lead to increased pH (Lager et al., 2006). As seen from the dissolution reactions, Equation 7 and 8, when carbonate dissolves there will be an excess of OH⁻. Cation exchange occurs between the clay and the injected water. At the clay surface adsorbed cations will be replaced by H⁺ in the fluid, leading to increased pH due to a decrease in H⁺-concentration (Lager et al., 2006).



Several experiments have been done on this, and it seems like pH increase is not the mechanism behind the LowSal effect, but more a result of LowSal waterflooding, increasing the oil recovery.

Multicomponent Ionic Exchange (MIE)

Lager et al. (2006) proposed that multicomponent ionic exchange (MIE) between clay mineral surfaces and the injected brine is responsible for the improvement in oil recovery when LowSal water is injected.

As showed in the Table 3-3, eight different mechanisms for adsorption of organic matter onto clays are suggested by Sposito (1989). The mechanisms are dependent on the condition of the clay surface and the organic function of the organic matter.

Table 3-3: Possible adsorption mechanisms between organic compounds onto clay minerals (Sposito, 1989).

<i>Mechanism</i>	<i>Organic functional group involved</i>
Cation exchange	Amino, ring NH, heterocyclic N (aromatic ring)
Protonation	Amino, heterocyclic N, carbonyl, carboxylate
Anion exchange	Carboxylate
Water bridging	Amino, Carboxylate, carbonyl, alcoholic OH
Cation bridging	Carboxylate, amines, carbonyl, alcoholic OH
Ligand exchange	Carboxylate
Hydrogen bonding	Amino, carbonyl, carboxyl, phenolic OH
Van der Waals interaction	Uncharged organic units

Among these mechanisms, it is suggested that one of the primary mechanisms causing the increased oil recovery from LowSal waterflooding, is the cation exchange between the clay surface and the injected water (Lager et al., 2006; Lager et al., 2008a). The different mechanisms are illustrated in Figure 3-17.

When polar compounds like resins and asphaltenes in the oil bonds with multivalent cations at the clay surface, and when organic polar compounds adsorbs directly onto clay mineral surfaces by displacement of the most unstable cations present at the clay surface, the reservoir rock becomes oil-wet. The polar compounds in the oil are attached to the negatively charged surface, and divalent cations like calcium and magnesium act as bridges between the negatively charged compounds in the oil and the negatively charged clay surface, illustrated in Figure 3-17. When LowSal brine is injected, the divalent ions exchange with either cationic organic compounds or with bases due to the change in ion exchange equilibrium. The consequence of this will be that the bonded oil will become mobile, wettability alters towards more water-wet and the oil recovery will increase (Lager et al., 2006; Lager et al. 2008a).

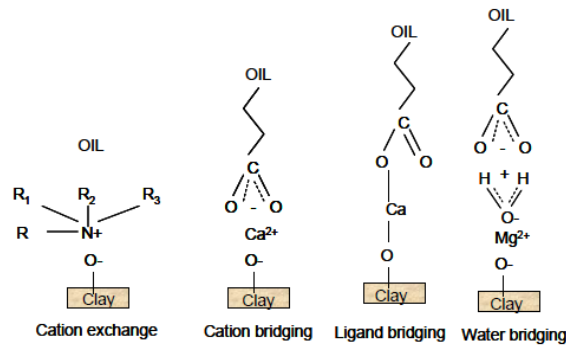


Figure 3-17: Clay/oil attraction by divalent cations (Lager et al., 2008a).

Furthermore, Lager et al. (2006) suggest that injecting LowSal water will change the charge density of the clay resulting in expansion of the electric double layer by the MIE mechanism and enabling desorption of the oil from the surface.

Double layer effect

Ligthelm et al. (2009) propose that the electrical double layer between the clay and the oil interfaces expands when the salinity decreases. The oil will detach from the surface and the wettability of the reservoir rock surface becomes more water-wet causing a LowSal effect. Similar to Figure 3-17, by Lager et al. (2008a), Ligthelm et al. (2009) suggests there is a Ca^{2+} bridge between the negatively charged clay and oil.

The expansion of the electrical double layer due to LowSal associated with MIE enables desorption of polar compounds from the clay surface. This results in an increase in oil recovery because the bonds holding oil in contact with the rock are broken (Lager et al., 2008a).

Salting-in Effect

RezaeiDoust et al. (2011) suggested that the main mechanism for LowSal effects was related to changes in the solubility of polar organic components in the aqueous phase, called a salting-in effect.

Organic material in water is solvated because the hydrogen bonds between water molecules form water structures around the hydrophobic part of the material. In high saline (HighSal) water, inorganic ions like Ca^{2+} , Mg^{2+} and Na^+ , will break up these water structures and consequently decrease the solubility. Furthermore, the organic material will move to and adsorb at the rock surface. Between the negatively charged clay surface and the organic material the cations create a bond, illustrated in Figure 3-18 (a). This mechanism is called a salting-out effect, where the solubility of organic material in water decreases by adding salt to the solution. LowSal water will have the opposite effect. By removing salt from the water, the solubility of organic material in water increases, and salting-in effect is obtained. When the salinity is below the critical ionic strength, the bond between the ions and the clay surface will weaken as a result of the decreased ionic strength in the water phase. Then, organic material will move away from the surface and desorb, contributing to the LowSal mechanism. This is illustrated in Figure 3-18 (b).

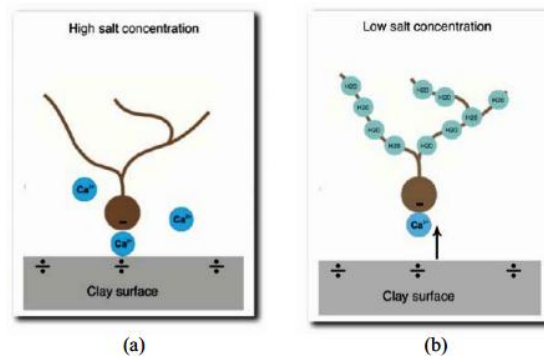


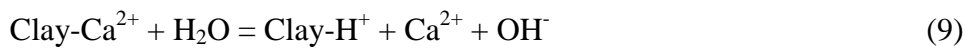
Figure 3-18: Illustration of (a) salting-out effect and (b) salting-in effect (Melberg, 2010).

This mechanism is not believed in any longer, as the adsorption studies show higher adsorption of polar organic material in LowSal brine, compared to HighSal.

Local pH increase

One of the latest suggested mechanisms of LowSal is desorption of acids and bases by pH increase made by Austad et al. (2010). The mechanism is illustrated in Figure 3-19. As mentioned in section 3.3.1, a structural imbalance in the silica or in the aluminum layer and

also at the edge surfaces, cause a negative charge on the clay surface. The clay minerals are therefore able to exchange cations adsorbed between their layers and to their external surfaces. At reservoir conditions, acidic and basic organic material is adsorbed onto the clay together with inorganic ions, especially Ca^{2+} , from the FW, and a chemical equilibrium is established. By injecting LowSal water this equilibrium is disturbed because of the difference in ion concentration between the injected water and the initial FW, leading to desorption of cations, especially Ca^{2+} . Protons, H^+ , from the water close to the clay surface, adsorb onto the clay and replace the Ca^{2+} . A local increase in pH close to the clay surface occurs, as illustrated by Equation 9 (Austad et al., 2010).



Because of the local increase in pH close to the clay surface, the adsorbed acidic and basic material reacts as in an ordinary acid-base proton transfer reaction, promoting desorption of organic material, water wetness increases and increased oil recovery is observed. The acid-base reaction takes place between the OH^- and the adsorbed acid and protonated base shown by Equation 10 and 11 (Austad et al., 2010).

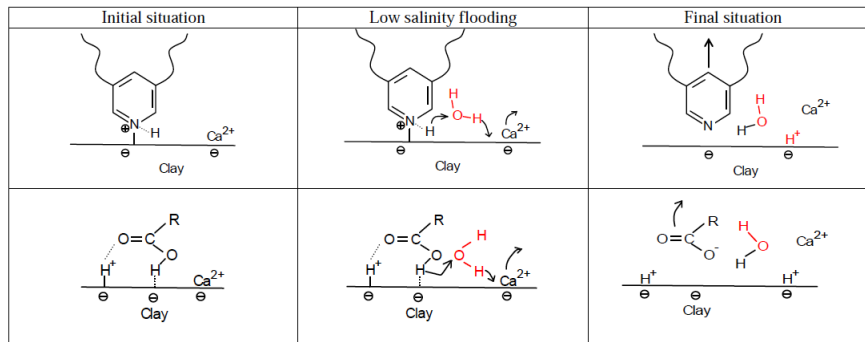
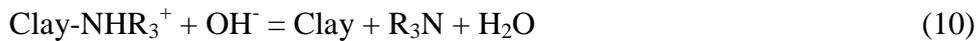


Figure 3-19: Illustration of the proposed mechanism for LowSal EOR effects (Austad et al., 2010). Upper: Desorption of basic material. Lower: Desorption of acidic material. Initial pH at reservoir conditions may be in the range of 5.

Adsorption of basic material

Several studies of the effect of pH on adsorption and desorption of organic compounds onto clay have been done. Burgos et al. (2002) performed an adsorption study of basic material (quinoline) onto kaolinite and montmorillonite in CaCl_2 solutions. Results from this study are illustrated in Figure 3-20 and 3-21, showing that the adsorption is a pH dependent process.

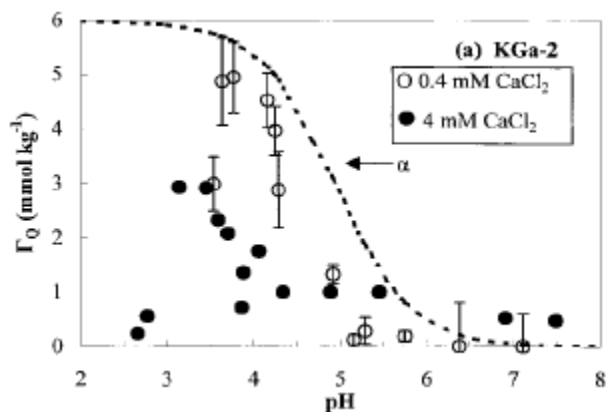


Figure 3-20: Adsorption of quinoline onto kaolinite (Burgos et al., 2002).

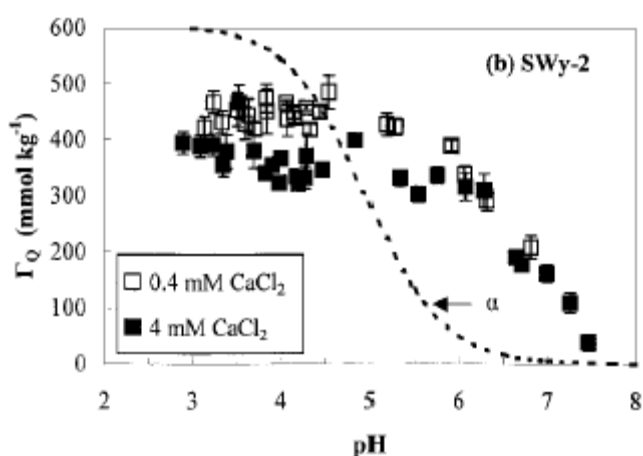


Figure 3-21: Adsorption of quinoline onto montmorillonite (Burgos et al., 2002).

The adsorption of quinoline decreased with increasing pH, and the largest adsorption was observed at a pH of 4. This decrease was more significant for kaolinite compared to montmorillonite. As the pH increased above 5, the adsorption of quinoline onto kaolinite was less than 1 mmol/kg, while at pH 7, the adsorption onto montmorillonite still was above 100 mmol/kg.

Studies done by Aksulu et al. (2012) on adsorption of quinoline onto illite in LowSal and HighSal brines are illustrated in Figure 3-22. As was expected, this study shows that the adsorption of basic material onto the clay was at maximum close to the pK_a value of quinoline. When pH is below the pK_a value the adsorption of quinoline to the clay surface decreases although the concentration of protonated quinoline increases. From Equation 1, H^+ has the highest affinity towards the clay surface which causes decreased adsorption of quinoline when the H^+ concentration increases. When pH is above the pK_a value less quinoline will adsorb to the clay surface due to the increase in the concentration of the neutral form quinoline. Figure 3-22 also illustrates that the adsorption of quinoline in the LowSal

brine is higher than for the HighSal brine. The reason for this is that there is a lower concentration of divalent cations, especially Ca^{2+} , in the LowSal brine which results in less competition between the cations and protonated quinoline.

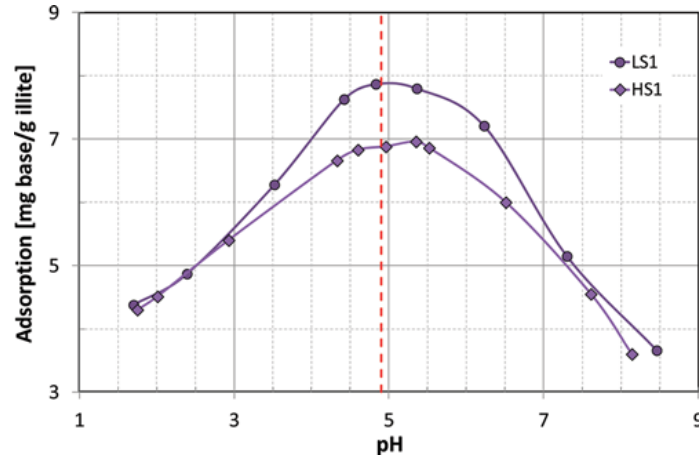


Figure 3-22: Adsorption of quinoline vs. pH at ambient temperature in LowSal brine (1000 ppm) and HighSal brine (25 000 ppm). The dashed line represents the pK_a value of quinoline.

Further, Burgos et al. (2002) found that the adsorption of quinoline onto kaolinite and montmorillonite also was affected by the concentration of Ca^{2+} . Increasing the concentration from 0.4 mM to 4.0 mM, in Figure 3-20 and 3-21, decreased the adsorption of quinoline onto the clay. Quinoline has pK_a value 4.9. The protonated quinoline, which is most reactive, competes with both Ca^{2+} and H^+ ions for the negative sites on the clay surface. Less protonated quinoline will adsorb when pH is below the pK_a value and concentration of Ca^{2+} and H^+ is high.

Adsorption of acidic material

Madsen and Lind (1998) performed an adsorption study of acidic material (benzoic acid) onto kaolinite in a NaCl solution. Also, results from this study show that the adsorption process is pH dependent. As illustrated in Table 3-4 the adsorption decreased with increasing pH.

Table 3-4: Adsorption of benzoic acid onto kaolinite using a 0.1 M NaCl solution at 32°C (Madsen & Lind, 1998).

$\text{pH}_{\text{initial}}$	Γ_{max} $\mu\text{mole}/\text{m}^2$
5.3	3.7
6.0	1.2
8.1	0.1

Benzoic acid has a pK_a value 4.4. When the pH is equal to this value the fraction of the neutral form of the carboxylic material becomes equal to the anionic form. Both the neutral and anionic form of the carboxylic material adsorbs to the clay surface when pH ranges from 4-5. Figure 3-23 illustrates the hydrogen bonding which forms between the oxygen of the carboxylic acid group and an adsorbed H^+ , and the proton of the carboxylic acid which attaches to a negatively charged site on the clay.

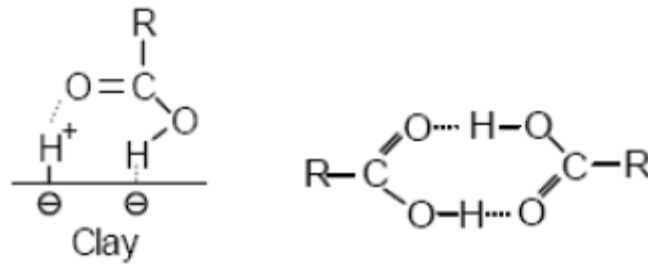


Figure 3-23: Supposed adsorption of carboxylic group onto clay by H-bonding (Austad et al., 2010).

Temperature and pH

A systematic study between temperature, pH gradient (ΔpH) and LowSal EOR effects on Berea core material showed a decreasing LowSal effect with increasing temperature, and a decreasing ΔpH when switching the flooding fluid from HighSal to LowSal (Gamage & Thyne, 2011). In line with these studies by Gamage and Thyne (2011), experimental work on a reservoir core from a high-temperature reservoir ($>100^\circ C$) containing HighSal FW ($>200\ 000$ ppm), done by Aksulu et al. (2012), also showed, and supported that there is a relationship between the temperature and ΔpH related to LowSal flooding, illustrated in Figure 3-24. At 40, 90, and $130^\circ C$ the order of the ΔpH was 2.6, 1.8, and 1.3, which means that when the temperature gets higher, Equation 9 moves to the left and a smaller ΔpH was observed. The reactivity of Ca^{2+} increases with increasing temperature which results in less adsorption of polar components onto the clay which can be seen from the experimental work by Håmsø (2011). Håmsø (2011) studied adsorption of quinoline onto illite in relation to LowSal flooding in ambient and high temperatures (above $100^\circ C$). The results from the adsorption of quinoline onto cleaned illite at ambient temperature are illustrated in Figure 3-25. The results supports that the adsorption is pH dependent. At $pH \sim 5$, the adsorption in the LowSal brine is higher than for the HighSal brine due to lower concentration of Ca^{2+} in the LowSal brine causing less competition between the cations and the protonated quinoline. The high adsorption for the Varg FW it not fully understood. Figure 3-26 illustrates the results at

a temperature of 130°C. Compared to ambient temperature, the adsorption is much lower which corresponds to a more water-wet system. Here, the adsorption for the LowSal water is higher than Varg FW which has higher concentration of Ca²⁺. The Ca²⁺ concentration is therefore an important parameter regarding high temperatures.

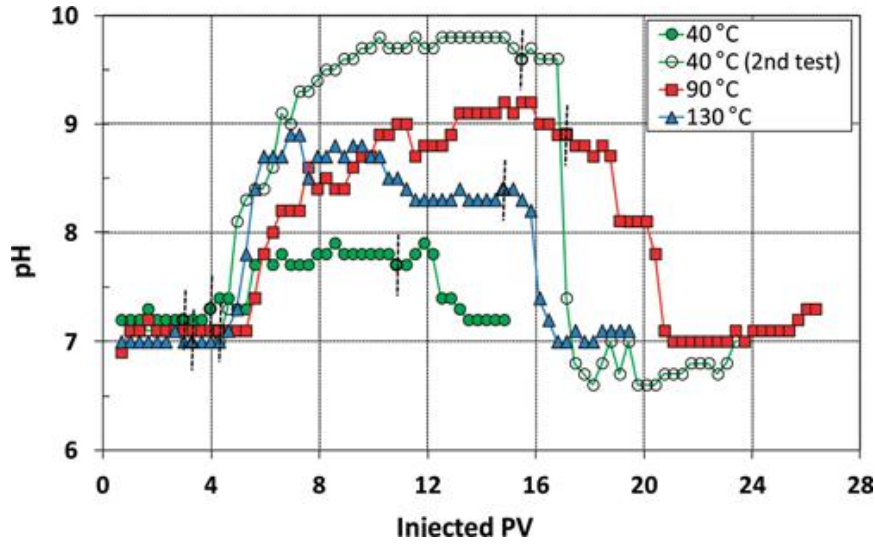


Figure 3-24: pH of effluent vs. injected PV for core RC1 at 40, 90, and 130 °C (Aksulu et al., 2012). The brine flooding sequence was HighSal-LowSal-HighSal. Dashed lines indicate switching of fluids.

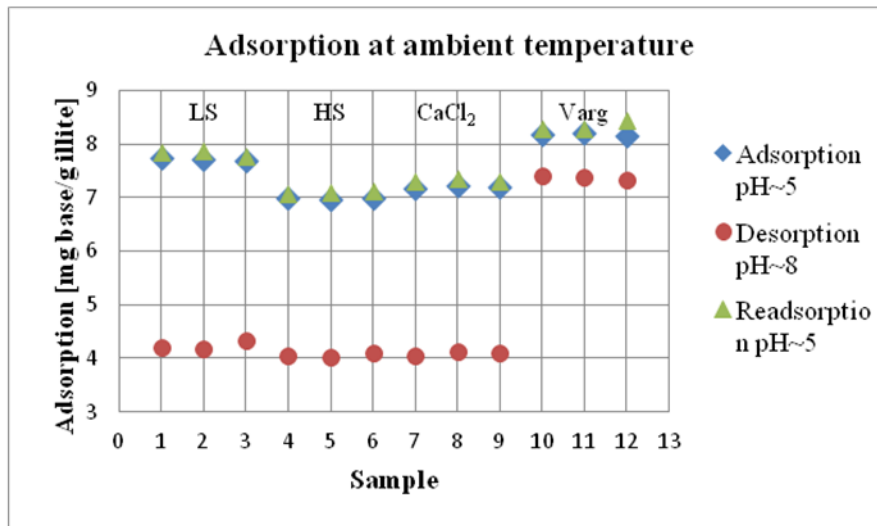


Figure 3-25: Adsorption of quinoline onto illite at ambient temperature using four different brines: LowSal, HighSal, pure CaCl₂ and Varg FW (Hamsø, 2011).

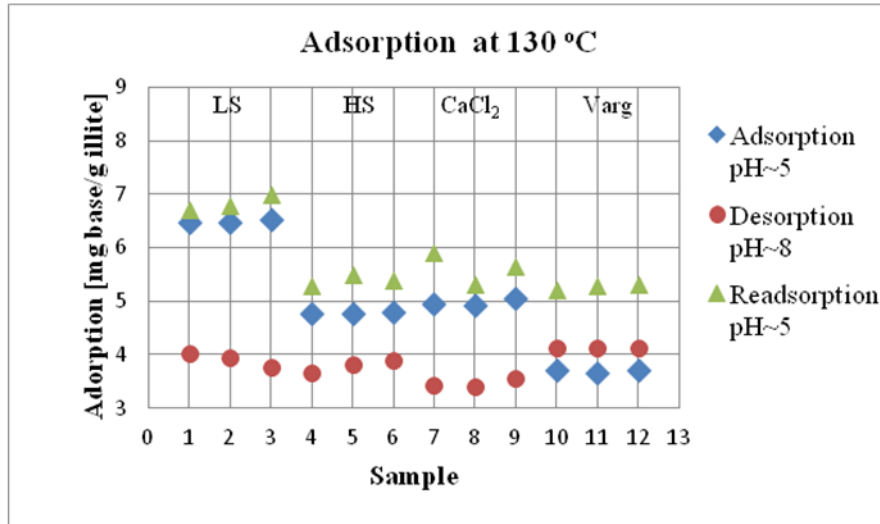


Figure 3-26: Adsorption of quinoline onto illite at 130 °C using four different brines: LowSal, HighSal, pure CaCl₂ and Varg FW (Hamsø, 2011).

Presence of Anhydrite

Illustrated by Equation 9, the presence of dissolvable salts of Ca²⁺ in the formation will affect desorption of active cations from the surface. Aksulu et al. (2012) work thereby concludes that the presence of anhydrite, CaSO₄, in an oil reservoir affect the LowSal EOR process. A reservoir containing dissolvable CaSO₄ will have a smaller ΔpH due to the increased solubility of CaSO₄ when injecting LowSal fluid. A small ΔpH will decrease desorption of active cations from the clay which means that the presence of CaSO₄ could prevent the LowSal effect. Also, the increasing temperatures and concentration of Ca²⁺, decreases the solubility of the CaSO₄ and results in precipitation of CaSO₄ from the formation. Constant pH and concentration of Ca²⁺ during LowSal flooding will not cause any dissolution of CaSO₄.

4 Experimental work

In this section the experimental materials used and experimental procedures will be described.

4.1 Materials

The basic materials used in this project were:

- Rock: One core plug from the Yme field.
- Oil: Crude oil from the Yme field.
- Brine: Four different brines for the main test.

4.1.1 Rock

A core plug is a cylindrical plug of rock cut from the location of the formation under study for use in laboratory tests and analyses (Aadnøy & Looyeh, 2011). In the experiment a sandstone core plug from the Yme field was selected, Yme Core#22. Figure 4-1 shows the sealed Yme Core#22. A cutting machine was used to cut the edges of the core so that it got a smooth surface at the ends to get full contact with the tubing and pieces in the core holder.

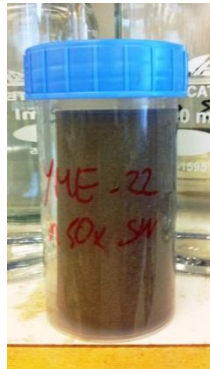


Figure 4-1: Sealed Yme Core#22.

The core was taken from well 9/2-7S, at a depth of 3917.85 m. The mineral composition of the core was measured with X-ray diffraction analysis (XRD), and provided by Talisman Energy. Table 4-1 lists the clay content and the complete XRD-analysis is shown in Appendix 1. It is assumed that the clay content for Yme Core#22 is in the area between the given depths. The core properties of Yme Core#22 are listed in Table 4-2. The measurements and calculations are provided in the experimental procedures in section 4.2.

Table 4-1: Clay content of Yme Core#22 is assumed to be in the range between the given depths.

Depth [m]	Illite/mica [wt%]	Kaolinite [wt%]	Chlorite [wt%]	Total Clay [wt%]
3917.75	7.4	9.6	1.5	18.5
3918.00	6.0	7.0	0.8	13.8

Table 4-2: Properties of Yme Core#22.

Yme Core#22	
L [cm]	7.685
D [cm]	3.780
V_b [cm ³]	86.24
W_s [g]	203.98
W_d [g]	190.39
W_{final} [g]	193.40
PV [cm ³]	13.21
Φ [%]	15.3
S_{wi} [%]	20

Where:

L = Length of core

D = Diameter of core

V_b = Bulk volume of core

W_s = Weight of core 100% saturated with diluted Yme FW

W_d = Weight of dry core

W_{final} = Final weight of core after desiccator

PV = Pore volume of core

Φ = Porosity of core

S_{wi} = Initial water saturation

4.1.2 Oil

In the experiment reservoir crude oil from the Yme field was used. Before use, the crude oil was centrifuged for 45 min and filtered, first with a 5 μm Millipore filter and then a 2 μm Millipore filter, to remove possible particles. Density, AN and BN were then measured, see Table 4-3. The crude oil was stored in a colored glass bottle, see Figure 4-2.

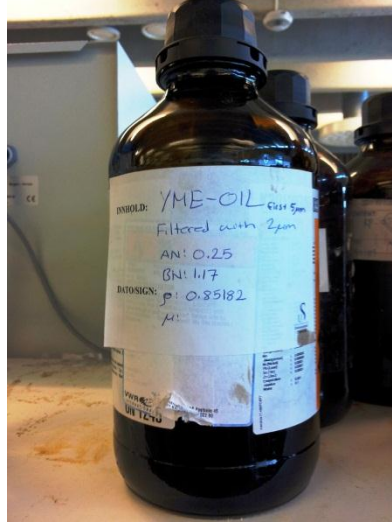


Figure 4-2: Yme Crude oil.

Table 4-3: Properties of Yme Crude Oil.

	AN [mg KOH/g]	BN [mg KOH/g]	Density [g/cm ³] 20°C
Yme Crude Oil	0.25	1.17	0.85182

4.1.3 Brines

The brines used in the main test were:

- Yme formation water (Yme FW)
- Synthetic seawater (SW)
- 50 times diluted seawater (d₅₀SW)
- Low Salinity Aluminum (LowSal Al)

The brines used for the experiments were prepared by dissolving different amounts of salts in distilled water to the compositions provided by Talisman Energy AS showed in Table 4-4. The complete tables of the compositions are found in Appendix 2. The solutions were stirred with a magnetic bar in a conical flask and then stored in clear glass bottles, see Figure 4-3 and 4-4. Some of the properties of the brines are showed in Table 3-5.

Table 4-4: Composition of brines.

Ions	Yme FW [mole/l]	SW [mole/l]	d ₅₀ SW [mmole/l]	LowSal Al 10 mM [mmole/l]
Cl ⁻	3.417	0.525	10.503	38.6
Mg ²⁺	0.080	0.045	0.891	-
Ca ²⁺	0.640	0.013	0.259	-
Na ⁺	1.915	0.450	9.002	8.6
K ⁺	0.033	0.010	0.201	-
Ba ²⁺	0.007	-	-	-
Sr ²⁺	0.008	-	-	-
HCO ₃ ⁻	-	0.002	0.040	-
SO ₄ ²⁻	-	0.0240	0.480	-
Al ³⁺	-	-	-	10.0
TDS [g/l]	195.68	33.39	0.668	1833
Ionic Strength	4.152	0.657	0.013	0.069



Figure 4-3: Stirring the solutions in a conical flask with a magnetic bar.



Figure 4-4: Clear bottles for storing.

Table 4-5: Properties of the brines.

Brine	Density [g/cm³]	Salinity [ppm]
Yme FW	1.13985	195 680
d ₅ Yme FW	1.02883	-
SW	1.024	33 390
d ₅₀ SW	1.024	668
LowSal AI	1.024	1 830
Distilled water	0.9982	0

Prior to use the brines were filtered through 0.22 μm Millipore filters to remove unsolvable particles, and vacuumed to remove any dissolved gas and prevent possible two phase flow inside the core during flooding.

4.2 Experimental procedures

4.2.1 Measurement of acid and base numbers

The AN and BN measurements of the oil were performed by using a titrating apparatus called “METTLER TOLEDO DL55 TITRATOR”, see Figure 4-5. Laboratory assistant, Hakan Aksulu, performed the AN and BN measurements by the use of the method developed by Fan and Buckley (2006).



Figure 4-5: The titrating apparatus for measuring AN and BN (Melberg, 2010).

4.2.2 Core cleaning

The core had to be cleaned for oil, formation brine and possible coring liquids before use in the experiment. The core was put inside a rubber sleeve and placed in a Hassler core holder, see Figure 4-6. In both ends of the core, inlet and outlet lines were attached, and a confining pressure of 30 bars was applied to the core from a nitrogen (N_2) tank. The purpose of this was to make sure that the core was only exposed to the cleaning fluid injected and to avoid fluid bypassing the core. In this stage the system was checked for possible leakages as well.



Figure 4-6: Hassler core holder (Melberg, 2010).

The different cleaning fluids used for the cleaning procedure were kerosene, toluene and methanol. They were put into piston cells and connected to the system, regulated by valves.

By injecting kerosene, oil and organic material was removed from inside the core. Kerosene was displaced when shifting to injecting toluene. The toxic toluene also dissolved the organic materials in the core. When the effluent toluene was clear, methanol was injected to displace the toluene, dissolving the salts and absorbing the water. At the end of the cleaning procedure 1000 ppm NaCl was used to remove the rest of the salt.

When changing to a new cleaning fluid, the clearness of the effluent was checked and air in the system was removed. This process was repeated for two weeks until the effluent was colorless and did not contain any oil. The injection rate used for the cleaning was 0.1 ml/min. Figure 4-7 show the core cleaning setup. The purpose of cleaning the core was to achieve a state that is as close to water-wet as possible.

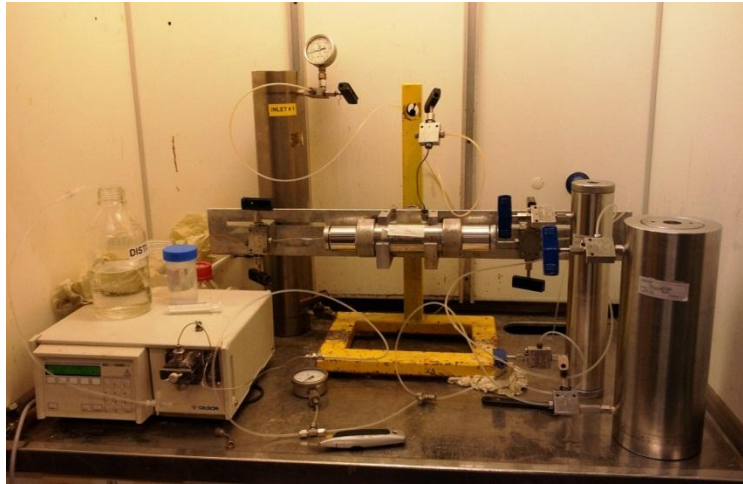


Figure 4-7: Core cleaning setup.

After the cleaning, the core was put into a heating chamber with a temperature of 90°C for drying. When dry, the length and diameter of the core was measured with a caliper and the core was weighed, see Table 4-2. These measurements were used when calculating the pore volume, porosity and initial water saturation of the core.

4.2.2.1 Removing CaSO_4

Yme Core#22 was also cleaned free of calcium sulfate (CaSO_4). This was done by flooding the core with 57PV of 1000 ppm sodium chloride (NaCl), and a batch test was performed. A batch test is "a laboratory testing procedure in which one test is done simultaneously on multiple specimens" (Lefers & the Holmgren Lab, 2004). By adding barium (Ba^{2+}) to the effluent, it was possible to check if the core was cleaned. Ba^{2+} reacts with SO_4^- and

precipitates as a white crystalline solid that is odorless and insoluble in water. When no precipitation in the effluent was observed, the core was clean from CaSO_4 .

4.2.3 Density measurement

The densities were measured by using a DMA 4500 Anton Paar Density Meter, shown in Figure 4-8.



Figure 4-8: A DMA 4500 Anton Paar Density Meter.

The measurements were done by injecting 2 ml of a sample into the density meter with a needle. It was important that the system was free of any air bubbles. The density meter performed the measurement and the value was given on the display. All measurements were done in 20°C. To remove oil or water/brine after each measurement, the system was cleaned with white spirit or acetone. White spirit removes oil, while acetone adsorbs water and dissolves white spirit.

4.2.3.1 Density of Yme FW and d_5 Yme FW

The density of the Yme FW and the five times diluted Yme FW (d_5 Yme FW) was measured twice, and the mean value of these measurements were used, see the following calculations. The density meter was cleaned with acetone. To calculate of the density of Yme FW, Equation 12 was used, while calculating of the density of d_5 Yme FW, Equation 13 was used.

$$\rho_{FW\#1} = 1.13989 \text{ g/cm}^3$$

$$\rho_{FW\#2} = 1.13980 \text{ g/cm}^3$$

$$\rho_{5xdFW\#1} = 1.02888 \text{ g/cm}^3$$

$$\rho_{5xdFW\#2} = 1.02878 \text{ g/cm}^3$$

$$\rho_{FW} = \frac{\rho_{\#1} + \rho_{\#2}}{2} \quad (12)$$

$$= \frac{1.13989 + 1.13980}{2} = \underline{1.13985 \frac{g}{cm^3}}$$

$$\rho_{5xdFW} = \frac{\rho_{\#1} + \rho_{\#2}}{2} \quad (13)$$

$$= \frac{1.02888 + 1.02878}{2} = \underline{1.02883 \frac{g}{cm^3}}$$

The density of the d₅Yme FW was used to calculate the pore volume and the porosity of the core, and the density of the Yme FW was used to calculate the final desired weight of the core.

4.2.4 Water saturation

When clean and dry, the core was put into a plastic container and connected to the water saturation system, see Figure 4-9. After vacuuming the core for three hours, the core was saturated with d₅Yme FW for three days.



Figure 4-9: Water saturation setup.

The weight of the 100% saturated core was 203.98 g, and it was used to calculate the pore volume and the porosity of the core.

4.2.5 Pore volume measurement

The pore volume calculation is based upon the weight difference between the dry and 100% saturated core, and the measured density of the d₅Yme FW. The pore volume of the core is expressed by Equation 14.

$$PV = \frac{W_s - W_d}{\rho_{5xdFW}} \quad (14)$$

Where:

PV = Pore volume of the core [cm^3]

W_s = Weight of core 100% saturated with d₅Yme FW [g]

W_d = Weight of dry core [g]

ρ_{5xdFW} = Density of d₅Yme FW [g/cm^3]

$$PV = \frac{203,98 \text{ g} - 190.39 \text{ g}}{1.02883 \text{ g/cm}^3} = 13.21 \text{ cm}^3$$

4.2.6 Porosity measurement

The porosity is a measure of the pore volume that is capable of holding fluids in a rock, and can be defined as the percentage of void per 100% volume of material. The porosity is denoted by φ and mathematically expressed by the Equation 15 (Dandekar, 2006). The bulk volume/total volume of the core was calculated by Equation 16.

$$\varphi = \frac{PV}{V_b} \times 100\% \quad (15)$$

Where:

φ = Porosity of core [%]

PV = Pore volume of core [cm^3]

V_b = Bulk volume of core [cm^3]

$$V_b = \pi hr^2 \quad (16)$$

V_b = Bulk volume of the core [cm^3]

h = Height of the core [cm]

r = Radius of the core [cm]

$$V_b = \pi \times 7.685 \text{ cm} \times (1.89 \text{ cm})^2 = 86.24 \text{ cm}^3$$

This gave that the porosity of the core was:

$$\varphi = \frac{13.21 \text{ cm}^3}{86.24 \text{ cm}^3} \times 100\% = \underline{15.3\%}$$

4.2.7 Initial water saturation

The initial water saturation of the core was decided to be lowered to 20%. The final weight of the 20% saturated Yme Core#22 was calculated by Equation 17.

$$W_{final} = W_d + 0.20 \times (PV \times \rho_{FW}) \quad (17)$$

Where:

W_{final} = Final desired weight of the core [g]

W_d = Weight of dry core [g]

PV = Pore volume of the core [cm³]

ρ_{FW} = Density of Yme FW at desired initial water saturation [g/cm³]

$$W_{final} = 190.39 \text{ g} + 0.20 \times (13.21 \text{ cm}^3 \times 1.13985) \text{ g} = \underline{193.40 \text{ g}}$$

This means that when the weight of the core was approximately 193.40 g, the goal of 20% saturated core was achieved. To make the core reach this final weight, 80% water had to be removed from the 100% saturated core. This was done by placing the core in a desiccator containing 20 g of silica gel, see Figure 4-10. The silica gel acts like a drying agent which evaporates and absorbs distilled water from the core, leaving the salts behind. During the next couple of days, 5-7 g of silica gel was added in the desiccator and the weight reduction of the core was monitored. When the core reached the final weight of 193.40 g, it was placed in a sealed plastic container and into the refrigerator to obtain uniform initial water saturation throughout the core.



Figure 4-10: Desiccator with Yme Core#22 and silica gel.

4.2.8 Asphaltene content

To measure the asphaltene content in the Yme crude oil, the standard procedure for separating asphaltenes from crude oils by Wang and Buckley (n.d.) was used. Content of asphaltene in the crude oil was measured by filtrating 20.227ml of the crude oil mixed with precipitant, in this case 80 ml of n-heptane. The separated asphaltene was dried and weighted. The total mass of the asphaltene was 0.2372 g. The amount of asphaltene was then calculated by Equation 18.

$$\begin{aligned} \text{Asphaltene content} &= \frac{\text{mass of dry asphaltene}}{\text{volume of crude oil}} & (18) \\ &= \frac{0.2372 \text{ g}}{20.227 \text{ ml}} = \underline{1.73 \frac{\text{g}}{100\text{ml}}} \end{aligned}$$

4.2.9 Oil saturation

When uniform initial water saturation throughout the core was obtained, it was placed in a Hassler core holder in a heating chamber. The temperature in the chamber was set to Yme reservoir temperature, 110°C, and the system was vacuumed for 20 minutes. In the meantime, Yme Crude oil was saturated with carbon dioxide (CO₂) at 2.5 bars in a recombination cell and connected to the system. When vacuum was achieved in the system, the core was flooded with the saturated Yme Crude oil. The core was flooded with 2PV of this oil in both directions. The core was now ready for ageing.

4.2.10 Aging of the core

The core was aged inside the Hassler core holder in the heating chamber for 14 days. The aging temperature was still equal to Yme reservoir temperature of 110°C, and the pressure set to 10 bars. The purpose of the aging process was to change the wettability of the core to a

more oil-wet condition, making the oil components adsorb onto the clay surface. This will make it possible to see a wetting alteration towards a more water-wet rock surface during the injection of water.

4.2.11 Waterflooding – main test

When the aging was completed, the core was ready for the waterflooding-test, which was the main test in this experiment, and the all of the main test data are found in Appendix 3.

The flooding setup consisted of the heating chamber with the Hassler core holder, piston cells, a Gilson 307 pump, pressure cylinders, a burette and a computer, see Figure 4-11. The piston cells contained the brines used for the flooding, and were connected to the Hassler core holder inside the heating chamber by steel pipes. The pump was connected to the computer. The pressure cylinders showed the confining pressure and the backpressure in the system. The confining pressure was used to give a good seal between the Hassler core holder and the rubber sleeve, and the backpressure was used to avoid any gas problems.

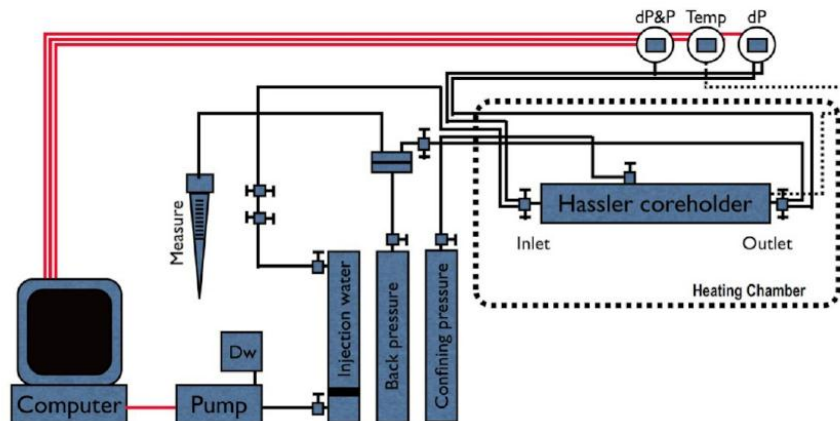


Figure 4-11: Waterflooding setup (RezaeiDoust et al., 2010).

The temperature was kept at the Yme reservoir temperature of 110°C and the confining pressure was set to 10 bars. The flow rate was set to $4PV = 0.037 \text{ ml/min}$, calculated by Equation 19.

$$\begin{aligned}
 \text{Flow rate} &= 4PV & (19) \\
 &= 4 \times \frac{PV}{t} \\
 &= 4 \times \frac{13.21 \text{ cm}^3}{1440 \text{ s}} = \underline{0.037 \text{ ml/min}}
 \end{aligned}$$

First, the core was flooded with Yme FW. When the oil production reached the plateau and the salinity stabilized, the core was flooded with SW. Again, when the salinity and pH were stabilized, the core was flooded with d₅₀SW. Finally, the core was flooded with LowSal A1 until salinity and pH stabilized again, and no oil production was observed.

During the flooding, the production fluids collected in the burette by the outlet was frequently drained, see Figure 4-12.



Figure 4-12: Burette with effluent water and oil.

The computer program registered the date, time, amount of brine injected, PV injected, produced oil and oil recovery when the samples were taken. Volume of produced liquids (effluent water and oil) and the pressure difference, ΔP , was recorded.

4.2.11.1 Density and pH measurements of effluent water

Both the pH and density of the samples of the effluent water were measured and logged in the computer program.

The densities were measured as described in section 4.2.3, and they were used to calculate the effluent salinities.

The pH was measured with a METTLER TOLEDO pH meter, see Figure 4-13. To measure the pH, 2 ml of the effluent water was needed. The electrode was cleaned with distilled water and water droplet wiped off before putting it into the effluent. Then it was stirred in the effluent until the pH was stabilized, and the pH was recorded in the computer program. The results are presented as plots of salinity and pH versus injected PV of brine in the result section 5.



Figure 4-13: METTLER TOLEDO pH meter.

4.2.11.2 Oil recovery calculation

The produced amount of oil was read off the burette and used to calculate the oil recovery. The oil recovery and original oil in place were calculated by Equation 20 and 21.

$$\text{Recovery [\%]} = (\text{Amount of oil produced}/\text{OOIP}) \times 100\% \quad (20)$$

$$\text{OOIP} = (1 - S_{wi}) \times \text{PV} \quad (21)$$

Where:

S_{wi} = Initial water saturation

PV = Pore volume of the core [ml]

The results are presented as plots of oil recovery versus injected PV of brine in the result section 5. The recovery factor was calculated by Equation 22.

$$R = \frac{V_{prod}}{OOIP} \times 100\% \quad (22)$$

Where:

R = Oil recovery factor [%]

V_{prod} = Volume of oil produced [ml]

$OOIP$ = Original oil in place [ml]

4.2.11.3 Volume correction: Shrinkage factor

An illustration of the setup for measurements of the volume correction is drawn in Figure 4-14. The recombination cell with oil saturated with CO_2 is connected to a MicoMotion

CMFS010, by Emerson, with a wire. This apparatus measured the densities. From the apparatus a line was leading to a container.

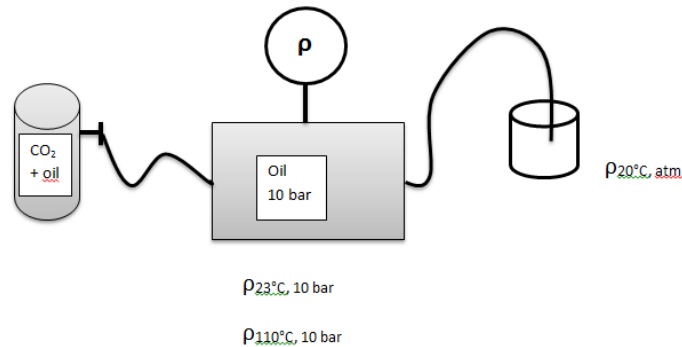


Figure 4-14: Illustration of the volume correction setup.

Shrinkage is a term used to describe the volume deficit between oil at reservoir conditions and atmospheric condition. Oil at 110°C and 10 bars will yield a completely different volume than oil at standard conditions.

CO₂-saturated oil entered the apparatus by the wire. The temperature was set to 110°C and the pressure to 10 bars inside the apparatus, and the density of the oil was displayed on the apparatus. The pressure remained at 10 bars but the temperature was dropped to 23°C, and the density was measured again. Then the oil traveled through the line and was released to atmospheric conditions, 20°C, and the density was measured manually. Through this system and temperature drop, the oil “shrinks”.

The measured densities were:

$$\rho_{110^{\circ}\text{C}, 10 \text{ bar}} = 0.764 \text{ g/cm}^3$$

$$\rho_{23^{\circ}\text{C}, 10 \text{ bar}} = 0.848 \text{ g/cm}^3$$

$$\rho_{20^{\circ}\text{C}, \text{atm}} = 0.852 \text{ g/cm}^3$$

The mass of the oil released to atmospheric conditions was measured:

$$m_{\text{oil}} = 7.0423 \text{ g}$$

The volume of the flashed oil was measured:

$$V_{\text{oil flashed}} = 8.626 \text{ ml}$$

The volume of the oil at standard condition was calculated by Equation 23.

$$V_{STD} = \frac{m_{oil}}{\rho} \quad (23)$$

$$= \frac{7.0423 \text{ g}}{0.852 \text{ g/ml}} = \underline{8.266 \text{ ml}}$$

The total shrinkage in the system is a summation of the shrinkage from $V_{110^\circ\text{C}} \rightarrow V_{23^\circ\text{C}}$ and from $V_{23^\circ\text{C}} \rightarrow V_{atm}$ was calculated by Equation 24 and 25, and the total shrinkage by Equation 26.

$$\text{Shrinkage from } V_{110^\circ\text{C},10\text{bar}} \rightarrow V_{23^\circ\text{C},10\text{bar}} = 1 - \frac{\rho_{110^\circ\text{C},10\text{bar}}}{\rho_{23^\circ\text{C},10\text{bar}}} \quad (24)$$

$$= 1 - \frac{0.764}{0.848}$$

$$= \underline{0.099}$$

$$\text{Shrinkage from } V_{23^\circ\text{C},10\text{bar}} \rightarrow V_{atm} = 1 - \frac{m_{oil}/\rho_{20^\circ\text{C},atm}}{V_{oil}} \quad (25)$$

$$= 1 - \frac{7.0423 \text{ g} / 0.852 \frac{\text{g}}{\text{cm}^3}}{8.266 \text{ ml}}$$

$$= \underline{0.042}$$

$$\text{Total Shrinkage} = \text{Shrinkage from } V_{110^\circ\text{C},10\text{bar}} \rightarrow V_{23^\circ\text{C},10\text{bar}} \quad (26)$$

$$+ \text{Shrinkage from } V_{23^\circ\text{C},10\text{bar}} \rightarrow V_{atm}$$

$$\text{Total shrinkage} = (0.099 + 0.042) \times 100\% = \underline{14.1\%}$$

4.2.11.4 Cation and anion content

The cation and anion content of the produced water was measured with a DIONEX ICS-3000 ion chromatograph, see Figure 4-15. Selected effluent samples from the waterflooding test were diluted and filtered, and put in the ion chromatograph in the correct order. The chromatograph was connected to a computer programmed to perform the measurements of the concentration of cations (calcium) and anion (sulphate).



Figure 4-15: The ICS-3000 ion chromatography (Dionex Corporation, 2006).

The results are presented as plots of calcium and sulfate content versus injected PV of brine in the result section 5. The data from the computer are found in the tables in Appendix 4.

4.2.12 Uncertainties in the experimental work

During the experimental work there was in almost every measurement both human and instrumental uncertainties present. There will always be some errors doing experimental work. Uncertainties are discovered when performing measurement several times on the same sample, and evaluating the difference in the results. By measuring the pH of the same sample several times, different values of the same sample indicate that uncertainty was related to the pH-electrode. It was also difficult to get an accurate reading of the produced oil in burette during the waterflooding part of the experiment which could have a great impact on the results.

5 Results

The main objective of the experimental work was to observe LowSal effects. The results from this experiment are compared with the results from a similar experiment on Yme Core#23 done by Master Student, Kine Navratil. Both cores are taken from the same well at approximately the same depth. Yme Core#22 was cleaned of CaSO₄, but Yme Core#23 was not. For both cores the aging and flooding temperature was 110°C, and the oil was saturated with CO₂. The test conditions are listed in Table 5-1. In the following sub-sections all the results are presented.

Table 5-1: Test conditions.

Test conditions	Yme Core#22	Yme Core#23
S _{wi} [%]	20	20
T _{aging} [°C]	110	110
T _{flooding} [°C]	110	110
Test sequence	FW - SW - d ₅₀ SW - LowSal Al	FW - SW - d ₅₀ SW

5.1 Yme Core#22

Yme Core#22, not containing CaSO₄, was flooded with formation water (FW), sea water (SW), fifty times diluted seawater (d₅₀SW) and Low Salinity Aluminum (LowSal Al) at a temperature of 110°C. Initial water saturation was 20%. Figure 5-1 shows the oil recovery (%OOIP) versus PV of brine injected and Figure 5-2 shows salinity and pH versus PV of injected brine. The complete data is found in Appendix 3.

Figure 5-3 shows the concentration of Ca²⁺ and SO₄²⁻ in the effluent versus PV of injected brine for Yme Core#22. The complete data is found in Appendix 4.

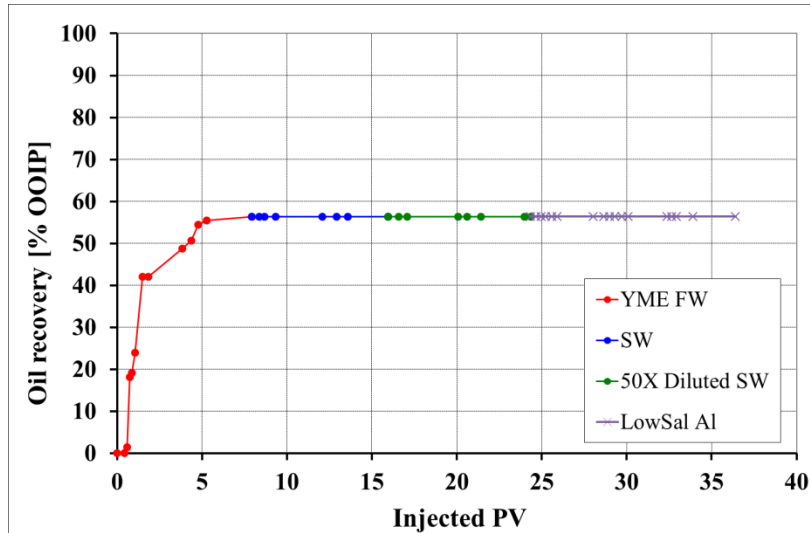


Figure 5-1: Oil recovery vs. PV of injected brine for Yme Core#22 at 110°C with injection rate 4PV/day.

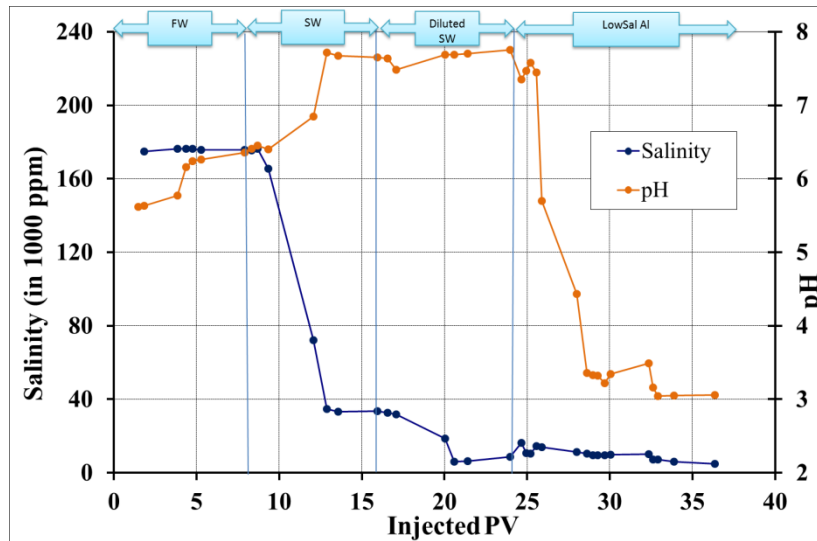


Figure 5-2: Salinity and pH vs. PV of injected brine for Yme Core#22, not containing CaSO₄.

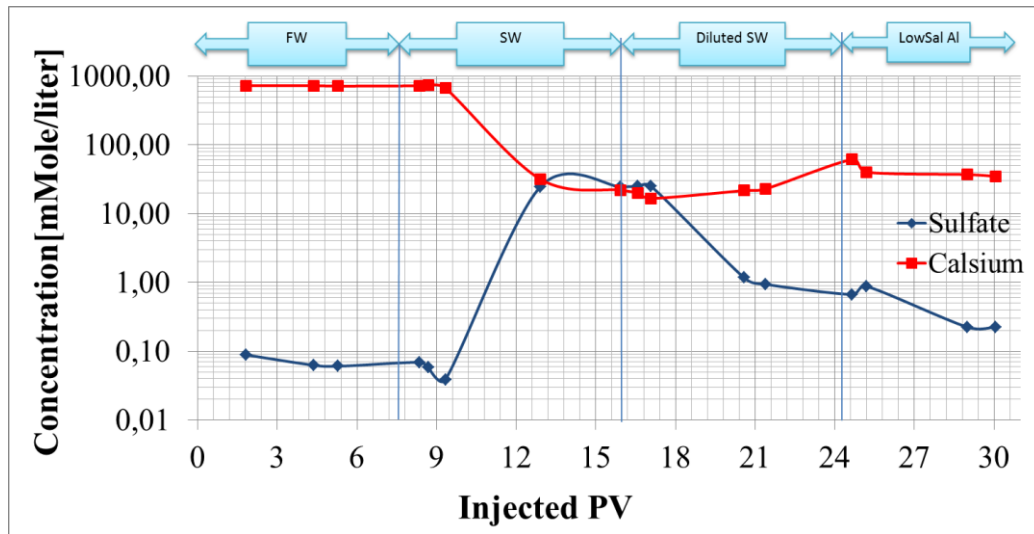


Figure 5-3: Concentration of Ca²⁺ and SO₄²⁻ in the effluent vs. PV of injected brine for Yme Core#22, not containing CaSO₄.

When FW was injected, there was a piston like displacement of oil up to 42 % recovery. After injecting 8 PV of FW, the oil recovery reached the plateau at 56.40 % of OOIP (corrected for shrinkage). The salinity of the effluent was stabilized on approximately 175 000 ppm during the injection of FW. Due to the CO₂ in the oil, the initial pH of the produced water was lowered to a value of 5.6. A pH increase up to 6.3 was observed during the FW flooding. The concentration of Ca²⁺ in the effluent was stable at a high value of 727 mMole/l when injecting FW. On the other hand, the concentration of SO₄²⁻ was low, 0.07 mMole/l during FW flooding.

After 8PV injection of SW started. No extra oil was produced during the injection. The pH increased by 1.4 pH units, and the salinity decreased to approximately 33 000 ppm. The concentration of Ca²⁺ decreased to 21.9 mMole/l, and stabilized during the injection, while the SO₄²⁻ concentration had a quick dip at first, but rose to 25 mMole/l.

The injection fluid was switched to d₅₀SW after 16PV was injected. Still, no extra oil was produced. No large change in pH was observed either, and the salinity decreased to 8 000 ppm. The concentration of Ca²⁺ was stable at 21.9 mMole/l, while the concentration of SO₄²⁻ decreases to 0.7 mMole/l.

Finally, LowSal AI was injected. No extra oil was produced. A quick increase to 16 000 ppm in salinity was observed, before it decreased again to 4 000 ppm. A large decrease of 4.7 pH units was observed during the injection of LowSal AI. The pH decreased below the initial pH of the LowSal AI brine of 4. Injecting LowSal AI resulted in an increase to 35 mMole/l of the concentration of Ca²⁺ while SO₄²⁻ decreased a little bit to 0.22 mMole/l. Both the concentrations stabilized at these values until the end of the flooding.

5.2 Yme Core#23

Yme Core#23 was flooded with formation water (FW), sea water (SW) and fifty times diluted seawater (d₅₀SW) at a temperature of 110°C. Figure 5-4 shows the oil recovery (% OOIP) versus PV of brine injected and Figure 5-5 shows salinity and pH versus PV of injected brine.

Figure 5-6 shows the concentration of Ca²⁺ and SO₄²⁻ in the effluent versus PV of injected brine for Yme Core#23.

The data are taken from work done by Navratil (2012).

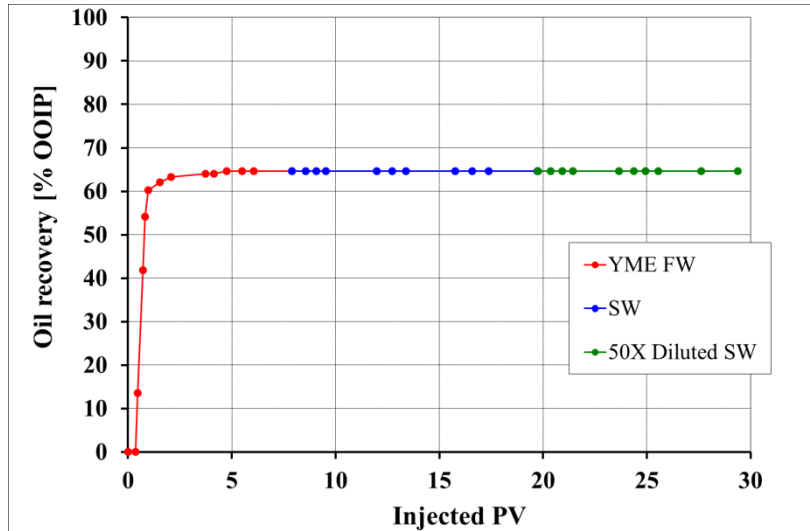


Figure 5-4: Oil recovery vs. PV of injected brine for Yme Core#23 at 110°C with injection rate 4PV/day.

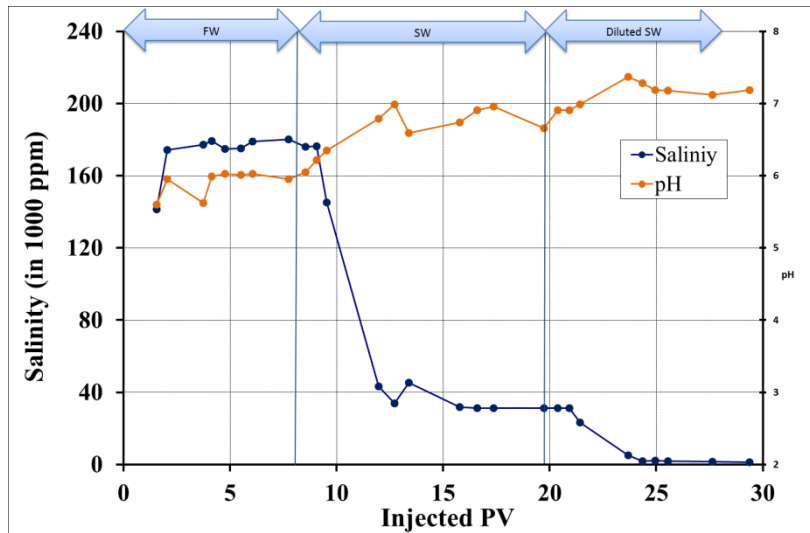


Figure 5-5: Salinity and pH vs. PV of injected brine for Yme Core#23.

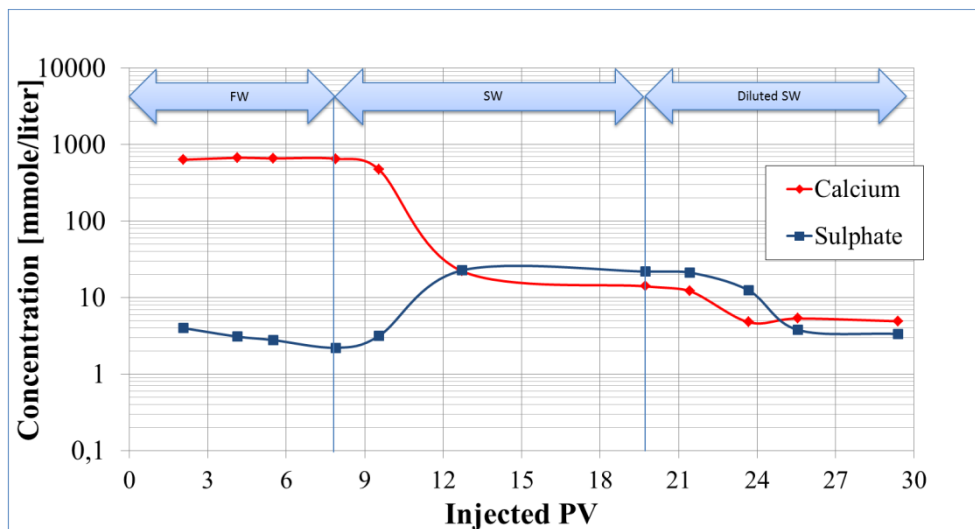


Figure 5-6: Concentration of Ca^{2+} and SO_4^{2-} in the effluent vs. PV of injected brine for Yme Core#23.

When FW was injected, there was a piston like displacement of oil up to 41 % recovery. After injecting 5 PV of FW, the oil recovery reached the plateau at 64.59 % of OOIP (corrected for shrinkage). The salinity of the effluent was stabilized on approximately 177 000 ppm during the injection of FW. Due to the CO₂ in the oil, the initial pH of the produced water was lowered to a value of 5.6. A pH increase up to 6 was observed during the FW flooding. The concentration of Ca²⁺ in the effluent was stable at a high value of 660 mMole/l when injecting FW. On the other hand, the concentration of SO₄²⁻ was low, 3 mMole/l during FW flooding.

After 8PV injection of SW started. No extra oil was produced during the injection. The pH increased by 1 pH units, and the salinity decreased to approximately 31 000 ppm. The concentration of Ca²⁺ decreased to 15 mMole/l, and stabilized during the injection, while the SO₄²⁻ concentration rose and stabilized at 22 mMole/l.

The injection fluid was switched to d₅₀SW after 20PV was injected. Still, no extra oil was produced. No large change in pH was observed either, and the salinity decreased to 1 300 ppm. The concentration of Ca²⁺ decreased and stabilized at 5 mMole/l, while the concentration of SO₄²⁻ decreased and stabilized at 4 mMole/l.

6 Discussion

In this section the main results from the experimental work in this thesis and the results from the “twin” core (Yme Core#23) done by Master Student, Kine Navratil, are compared. The results from the experiments are related to the new suggested mechanism of LowSal, concerning desorption of acids and bases by a local increase in pH.

Yme Core#22 and Yme Core#23 are assumed to have almost the same clay content because they are taken from the same well, only a couple of meters apart. For both cores, the aging and flooding temperature was 110°C and the oil was saturated with CO₂ to make the conditions as close as possible to what they experienced in the reservoir. The cores were cleaned, an initial water saturation of 20 % was established by desiccator, and the cores were saturated with the oil, 2PVs in each direction, and aged for 14 days. The flooding sequence was FW-SW-d₅₀SW for both cores. The main difference was that Yme Core#22 initially was cleaned free from CaSO₄ and also flooded with LowSal Al at the end of the waterflooding sequence.

The criteria for observing LowSal effects from the experiments should be in place. Yme crude oil had acid number 0.25 mg KOH/g and base number 1.17 mg KOH/g. This indicates that there is enough basic material to adsorb onto the surface of the clay. There was also a proper amount of clay content in both cores to get a LowSal effect. The clay content in both cores was relative high, assumed between 13.8-18.5 wt%.

The new mechanism relates the initial pH to the adsorption of polar components. Saturating the oil with CO₂ lowered the initial pH to 5.6 for both cores. This caused adsorption of polar components from the crude oil together with inorganic ions, Ca²⁺ from the FW, onto the negatively charged clay, resulting in an oil wet condition. Equilibrium was established.

This equilibrium was disturbed when LowSal water with ion composition different from the initial FW, was injected. The concentration of Ca²⁺ in the FW was higher than the concentration in the LowSal brines. When switching from HighSal to LowSal brine there was less competition between the cations and protonated basic material which caused an increase in the adsorption of polar components from the crude oil onto the clay. Ca²⁺ desorbed and was replaced by H⁺ close to the clay surface to balance the negative charge, resulting in a local increase in pH, as illustrated by Equation 9. An ordinary acid-base proton transfer reaction, Equation 10 and 11, occurred between the polar materials by the pH increase

causing desorption of organic material and a more water-wet condition. An increase in oil recovery should therefore be observed, but this was not the case.

For both experiments the pH increased with decreasing salinity. The pH of the produced water from the cores are shown in Figure 5-2 and 5-5. An increase is observed at the start of the flooding of HighSal water for both cores. For Yme Core#22, the effluent pH increased from 5.6 and stabilized at approximately 6.3. LowSal water increased the pH to 7.7. A large decrease in pH when injecting LowSal Al was observed due to the bonding of OH⁻ by Al³⁺. The pH went from 7.7 to 3.0, where it stabilized. For Yme Core#23 the initial pH of the produced water was lowered to a value of 5.6 due to the dissolved CO₂. When injecting FW the pH stabilized at 6 until the injection of SW. Then it increased to 7.0. Changing to d₅₀SW made the effluent pH stabilized around 7.1.

A typical observation during LowSal flooding experiments is an increase in pH of 1-3 units, which is related to the adsorption of polar material onto the clay. As mentioned, for Yme Core#22 and Core#23 a rather small increase of 1.4 and 1.0 was observed when switching the injected water from FW to SW, and an even smaller, almost unnoticeable when switching to a more LowSal water. The reason for observing a small ΔpH can be related to the high temperature used in the experiments. Under reservoir conditions the temperature is very high, here 110 °C. At high temperatures Equation 9 moves to the left, resulting in adsorption of polar components onto the clay together with inorganic ions, Ca²⁺. The purpose of injecting aluminum was to lower the pH, which was observed for Yme Core#22, and hopefully this result in higher adsorption of organic material onto the clay. A less water-wet system would led to better sweep efficiency, less snap-off oil, and increase the oil recovery.

The ΔpH for Yme Core#23 was smaller than for Yme Core#22. The reason for this was probably that Yme Core#23 contained CaSO₄. The smaller ΔpH was due to the increased solubility of CaSO₄ when LowSal fluid was injected. The desorption of active cations from the clay decreased and therefore, the presence of CaSO₄ may have prevented the LowSal effect, and no increased oil recovery. When flooding Yme Core#23 with d₅₀SW the concentration of Ca²⁺ in the effluent was therefore quite small. Combined with the high temperature in the experiment, this indicated that CaSO₄ precipitated from the core.

For both the cores the Ca²⁺ concentration in the effluent decreased and stabilized when injecting LowSal water, see Figure 5-3 and 5-6. For Yme Core#22, the Ca²⁺ concentration stabilized at 21.9 mMole/l when injecting d₅₀SW and then at 35 mMole/l when injecting

LowSal Al. For Yme Core#23, the concentration of Ca^{2+} stabilized at 5 mMole/l when injecting d_{50}SW . The decreased Ca^{2+} concentration in the effluent was related to the increase in pH which caused Ca^{2+} to adsorb onto the clay.

The oil recovery for the two cores is compared in Figure 6-1. First, the displacement of oil was more piston like for Yme Core#23, and therefore maybe acted more water-wet than Yme Core#22. Yme Core#23 reached the plateau at 64.59 % OOIP after injecting 5 PV, while Yme Core#22 reached its plateau at 56.40% OOIP after injecting 8 PV. Also, it was observed that Yme Core#23 had 8 % higher recovery than Yme Core#22. This was not an expected result because Yme Core#22 was cleaned for CaSO_4 and was expected to have a higher recovery due to higher desorption of cations from the surface with injection of d_{50}SW . When switching from HighSal to LowSal brine, no extra oil was recovered, which mean that no LowSal effect was observed in the experiments.

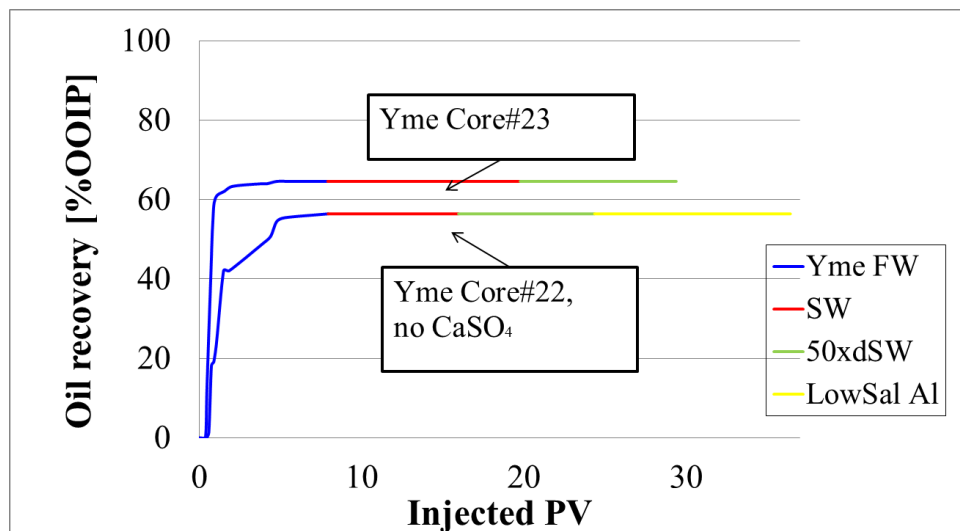


Figure 6-1: Comparison of the oil recovery for Yme Core#22 and Core#23.

Although the results from the “twin” cores are assumed to some extent be comparable, it is possible that this is not reasonable. The fact that the cores are from the same well and close by each other, the properties may be different. Some of their properties are listed in Table 6-1. These show that there is a difference in the PV of the cores. Yme Core#22 has a PV of 13.21 ml, while Yme Core#23 has a PV of 9.817 ml. Although the cores seem to have the same properties, the comparison of the two cores may however not be fair. The cores may act differently to the different brines which may be one reason for not getting the expected higher recovery when injecting LowSal brine. The interactions between the oil, brine and rock is complicated and play an important role. Adsorption of basic material onto illite, shown in

Figure 3-26, clearly showed that high temperature and HighSal (Varg FW) decreased the adsorption of the basic material. This is probably the case in this Yme experiment too. Low adsorption of polar components in the oil results in a water-wet system instead of partly oil-wet, which is preferable. If oil does not adsorb onto the clay, injecting LowSal water will not have any oil to displace, and no increase in oil recovery will be observed.

Table 6-1: Comparison of some of the core properties.

Core #	Φ [%]	PV [ml]	S_{wi} [%]	T_{aging} [°C]	$T_{flooding}$ [°C]	Q [PV/d]
22	15.3	13.21	20	110	110	4
23	15.3	9.186	20	110	110	4

7 Conclusions

The overall goal of this thesis was to observe LowSal effect and contribute with useful information to further research on the LowSal mechanism. Two sandstone cores from the Yme field were tested. One core containing anhydrite was flooded with FW, SW and d₅₀SW, while the other core not containing anhydrite was flooded with FW, SW, d₅₀SW and LowSal Al. For both cores the initial water saturation was 20%, the aging and flooding were performed at reservoir temperature, 110°C, and the crude oil was saturated with CO₂ to lower the pH of the FW during aging. The main conclusions from the experimental work are:

- The oil recovery was 56.40 % and 64.59 % of OOIP for Yme Core#22 and Yme Core#23, respectively. It was expected that Yme Core#22, not containing any CaSO₄, would have the highest oil recovery, but this was not the case.
- There were no signs of extra oil by switching from HighSal brine to LowSal brine during the waterflooding, which means that no LowSal effect was observed in the experiments.
- The reason for not obtaining any increased oil recovery in this experiment may be because the high temperature and HighSal water decreased the adsorption of the basic material. Low adsorption of polar components in the oil results in a water-wet system instead of partly oil-wet, which is preferable. If oil does not adsorb onto the clay, injecting LowSal water will not have any oil to displace, and no increase in oil recovery will be observed.
- An increase in pH of 1.4 and 1.0 units was observed when switching to SW for Yme Core#22 and Core#23. For Yme Core#22 the pH dropped below the initial value when switching to LowSal Al.
- The adsorption of polar material onto clay was dependent of the pH, temperature and Ca²⁺ concentration.
- The presence of CaSO₄ in the formation affected ΔpH and desorption rate of Ca²⁺, and therefore also the LowSal effect.
- Since it is difficult to draw any conclusions from this work because the mechanism of LowSal EOR is not fully understood, further studies have to be done. Future research could include experimental work where LowSal Al is injected at an earlier stage in the waterflooding.

8 Abbreviations

AN	Acid Number
BN	Base Number
CEC	Cation Exchange Capacity
d ₅₀ SW	Fifty times diluted seawater
EOR	Enhanced Oil Recovery
FW	Formation Water
HC	Hydrocarbons
HighSal	High Salinity
IFT	Interfacial Tension
IOR	Improved Oil Recovery
LowSal	Low Salinity
MIE	Multicomponent Ionic Exchange
OOIP	Original Oil In Place
SW	Sea water
XRD	X-Ray Diffraction

9 References

Aadnøy, B.S. and Looyeh, R., 2011. *Petroleum rock mechanics: drilling operations and well design*. Elsevier Gulf Professional Publishing, Amsterdam.

Ahmed, T.H., 2001. *Reservoir Engineering Handbook*. Second Edition. Gulf Professional Publishing, Boston.

Aksulu, H., Håmsø, D., Strand, S., Puntervold, T. and Austad, T., 2012. *Evaluation of Low-Salinity Enhanced Oil Recovery Effects in Sandstone: Effects of the Temperature and pH Gradient*. Energy & Fuels (in press).

Annual Information Form of Talisman Energy Inc., 2011, viewed 24th of April 2012, <http://www.talisman-energy.com/upload/media_element/20120312183646/Annual%20Information%20Form.pdf>.

Archer, J.S. and Wall C.G., 1999. *Petroleum Engineering – Principles and Practice*. Kluwer Academic Publishers.

Austad, T., RezaeiDoust, A. and Puntervold, T., 2010. *Chemical Mechanism of Low Salinity Water Flooding in Sandstone Reservoirs*. SPE 129767 prepared for presentation at the 2012 SPE Improved Oil Recovery Symposium, Tulsa, Oklahoma, USA.

Bavière, M., 1991. *Basic concepts in enhanced oil recovery processes*. Critical reports on applied chemistry, Volume 33. Published for the Society of Chemical Industry by Elsevier Applied Science.

Buckley, J.S and Liu, Y., 1998. *Some mechanisms of crude oil/brine/solid interactions*. Journal of Petroleum Science and Engineering 20(1998), 155-160.

Burgos, W.D., Pisutpaisal, N., Mazzaresse, M.C. and Chorover, J., 2002. *Adsorption of Quinoline to Kaolinite and Montmorillonite*. Environmental Engineering Science, 19(2): 59-68.

Cossé, R., 1998. *Basics of reservoir engineering*. Technip, Paris.

Dandekar, A.Y., 2006. *Petroleum reservoir rock and fluid properties*. Taylor & Francis, Boca Raton, Fla.

Darley, H.C.H. and Gray, G.R., 1988. *Composition and properties of drilling and completion fluids, 5th edition.* Gulf Publishing Company.

Dionex Corporation, 2006. *ICS-3000 Ion Chromatography System*, viewed 16th of April 2012, <http://www.dionex.com/en-us/webdocs/25859-ICS-3000_DataSheet_V30_releasedJC061506.pdf>.

Fan, T. and Buckley, J.S., 2006. *Acid number measurements revisited.* SPE 99884 presented at SPE/DOE Symposium on Improved Oil Recovery, Tulsa, OK, April 22–26, 2006.

Fanchi, J.R., 2010. *Integrated reservoir asset management: principles and best practices.* Elsevier Gulf Professional Publishing, Amsterdam, Burlington, Mass.

Gamage, P. and Thyne, G., 2011. *Systematic investigation of the effect of temperature during aging and low salinity flooding of Berea sandstone and Minn.* Proceedings of the 16th European Symposium on Improved Oil Recovery. Cambridge, U.K., April 12-14.

Green, D.W. and Willhite, G.P., 1998. *Enhanced oil recovery.* SPE Textbook Series, Volume 6. Society of Petroleum Engineers. Richardson, TX, USA.

Håmsø, D., 2011. *Adsorption of quinoline onto illite at high temperature in relation to low salinity waterflooding in sandstone reservoirs.* Master Thesis, University of Stavanger.

IDF, 1982. *Technical Manual for Drilling, Completion and Workover Fluids.* International Fluids Limited (Clay Chemistry), (Reprint 1/1992).

Jadhunandan, P.P. and Morrow, N.R., 1995. *Effect of Wettability on Waterflood Recovery for Crude Oil/Brine/Rock Systems.* Volume 10, Nr.1, SPE Reservoir Engineering, 40-46.

Jerauld, G.R., Lin, C.Y., Webb, K.J., and Secombe, J.C., 2008. *Modeling Low-Salinity Waterflooding.* SPE Reservoir Evaluation & Engineering, Volume 11, Nr.6., 1000-1012. SPE 102239-PA.

Lager, A., Webb, K.J., Black, C.J.J., Singleton, M. and Sorbie, K.S., 2006. *Low Salinity Oil Recovery – An Experimental Investigation.* SCA2006-36. Paper prepared for presentation at the International Symposium of the Society of Core Analysts held in Trondheim, Norway 12-16 September, 2006.

Lager, A., Webb, K. J., Collins, I. R., and Richmond, D. M., 2008a. *LoSalTM Enhanced Oil Recovery: Evidence of Enhanced Oil Recovery at the Reservoir Scale*, SPE 113976. Paper prepared for presentation at the 2008 SPE/DOE Improved Oil Recovery Symposium held in Tulsa, Oklahoma, USA, 19-23 April 2008.

Lager, A., Webb, K.J., Black, C.J.J., Singleton, M. and Sorbie, K.S., 2008b. *Low salinity oil recovery – an experimental investigation*. *Petrophysics*, 49(1): 28-35.

Ligthelm, D.J., Gronsveld, J., Hofman, J.P., Brussee, N.J., Marcelis, F., and van der Linde, H.A., 2009. *Novel Waterflooding Strategy by Manipulation of Injection Brine Composition*. SPE 119835. Paper prepared for presentation at the 2009 SPE EUROPEC/EAGE Annual Conference and Exhibition held in Amsterdam, The Netherlands, 8-11 June 2009.

Lefers, M. and the Holmgren Lab, 2004. *Batch testing - Definition*, viewed 24th of April 2012, <http://groups.molbiosci.northwestern.edu/holmgren/Glossary/Definitions/Def-B/batch_testing.html>.

Madsen, L. and Lind, I., 1998. *Adsorption of carboxylic acids on reservoir minerals from organic and aqueous phase*. *SPE Reservoir Evaluation & Engineering*, February: 47-51.

McGuire, P.L., Chatham, J.R., Paskvan, F.K., Sommer, D.M. and Carini, F.H., 2005. *Low Salinity Oil Recovery: An exciting new EOR opportunity for Alaska's North Slope*. Paper: SPE 93903 presented at the 2005 SPE Western Regional Meeting, Irvine, CA, USA, March 30 to April 1, 2005.

Melberg, E., 2010. *Experimental study of low salinity EOR effects from the Varg field*. Master Thesis, University of Stavanger.

Morad, S. and Worden, R.H., 2003. *Clay mineral cements in sandstones*. Special publication of the International Association of Sedimentologists. Blackwell, Oxford.

Navratil, K., 2012. *An Experimental Study of Low Salinity EOR effects on a core from the Yme field*. Master Thesis, University of Stavanger.

Oljedirektoratet, 2011. *Publikasjoner: Faktaheftet-Yme*, viewed 23rd of April 2012, <<http://www.npd.no/publikasjoner/faktahefter/fakta-2011/kap-11/yme/>>.

- Pu, H., Xie, X., Yin, P. and Morrow, N.R., 2008.** *Application of Coalbed Methane Water to Oil Recovery from Tensleep Sandstone by Low Salinity Waterflooding.* SPE/DOE Symposium on Improved Oil Recovery. Society of Petroleum Engineers, Tulsa, Oklahoma, USA.
- RazaeiDoust, A., 2011.** *Low Salinity Water Flooding in Sandstone Reservoirs – A Chemical Wettability Alteration Mechanism.* Ph.D. Thesis, University of Stavanger.
- RezaeiDoust, A., Puntervold, T., Strand, S. and Austad, T., 2009.** *Smart Water as Wettability Modifier in Carbonate and Sandstone: A Discussion of Similarities/Differences in Chemical Mechanisms.* Energy & Fuels, Paper: 23, 4479-4485.
- RezaeiDoust, A., Puntervold, T. and Austad, T., 2010.** *A Discussion of the Low Salinity EOR Potential for a North Sea Sandstone Field.* SPE134459, Prepared for presentation for the SPE Annual Technical Conference and Exhibition held in Florence, Italy, 19-22 September 2010.
- RezaeiDoust, A., Puntervold, T. and Austad, T., 2011.** *Chemical Verification of the EOR Mechanism by using Low Saline/Smart Water in Sandstone.* Energy & Fuels, Paper: 25, 2151-2162.
- Schlumberger Oilfield Glossary, 2012.** *The Oilfield Glossary: Where the Oil Field Meets the Dictionary*, viewed 5th of June 2012, <<http://www.glossary.oilfield.slb.com/>>.
- Skauge, A., Fallah, S. and McKay, E., 2008.** *Modeling of LPS Linked Polymer Solutions.* The 29th IEA Workshop & Symposium, Beijing, China.
- Sposito, G., 1989.** *The Chemistry of Soils.* Oxford University Press, New York.
- Strand, S., 2005.** *Wettability alteration in chalk, a study of surface chemistry.* Ph.D thesis, University of Stavanger.
- Strand, S., Puntervold, T. and Austad, T., 2012.** *EOR by Smart Water in Sandstones.* Unpublished material from the student meeting, mars 2012.
- Tang, G.Q., 1998.** *Brine Composition and Waterflood Recovery for Selected Crude Oil/brine/rock Systems.* Ph.D. Thesis, University of Wyoming.

Tang, G.Q. and Morrow, N.R., 1999. *Influence of Brine Composition and Fines Migration on Crude Oil/Brine/Rock Interactions and Oil Recovery.* Journal of Petroleum Science and Engineering, 24(1999), 99-111.

The NPD's Fact-pages, 2012. *Field: Yme, Well: 9/2-7S*, viewed 23rd of April 2012, <<http://factpages.npd.no/factpages/default.aspx?culture=en>>.

Wang, J. and Buckley, J., n. d. *Standard Procedure for Separating Asphaltenes from Crude Oils*, viewed 15th of May 2012, <http://baervan.nmt.edu/Petrophysics/group/prrc_02-02.pdf>.

Webb, K.J., Lager, A. and Black, C.J.J., 2008. *Comparison of high/low salinity water/oil relative permeability.* Paper: SCA2008-39 presented at the International Symposium of the Society of Core Analysts, Abu Dhabi, U. A. E., October 29- November 2.

Zolotukhin, A. B. and Ursin, J. R., 2000. *Introduction to Petroleum Reservoir Engineering.* Høyskoleforlaget AS, Kristiansand.

Appendices

Appendix 1: Composition of the rock

Table A-1.1: X-Ray Diffraction for well 9/2-7 S provided by Talisman Energy AS. The mineral composition for Yme Core#22 is assumed to be between the given depths.

Depth [m]	Illite/mica [wt%]	Kaolinite [wt%]	Chlorite [wt%]	Quartz [wt%]	Feldspar [wt%]	Plagioclase [wt%]	Calcite [wt%]	Dolomite [wt%]	Pyrite [wt%]	Total [wt%]
3917.75	7.4	9.6	1.5	68.5	1.6	9.3	0.6	0.9	0.6	100
3918.00	6.0	7.0	0.8	76.3	2.9	5.3	1.1	0.0	0.6	100

Appendix 2: Compositions of Brines

Table A-2.1: Composition of synthetic Yme formation water, Yme FW.

Salt	m [g/l]	m [mole/l] (molar)
	228.49	-
NaCl	111.92	1.915
KCl	2.43	0.033
MgCl ₂	7.605	-
CaCl ₂ (dry)	71.06	-
BaCl ₂	1.36	-
SrCl ₂	1.3	-
MgCl ₂ × 6H ₂ O	16.24	0.080
CaCl ₂ × 2H ₂ O	94.12	0.640
BaCl ₂ × 2H ₂ O	1.60	0.007
SrCl ₂ × 6H ₂ O	2.19	0.011
Density	1.006	-
Weight %	19.68	-
TDS	195.68	-
Ionic Strength	-	4.152
Ions	m [g/l]	m [mole/l] (molar)
Cl ⁻	12116	3.417
Mg ²⁺	1.94	0.080
Ca ²⁺	25.66	0.640
Na ⁺	44.03	1.915
K ⁺	1.27	0.033
Ba ²⁺	0.90	0.007
Sr ²⁺	0.72	0.008

Table A-2.2: Composition of synthetic seawater, SW.

Salt	m [g/l]	m [mole/l] (molar)
SSW	38.67	-
NaCl	23.38	0.400
Na ₂ SO ₄	3.41	0.024
NaHCO ₃	0.17	0.002
KCl	0.75	0.010
MgCl ₂	4.24	-
CaCl ₂ (dry)	1.44	-
MgCl ₂ × 6H ₂ O	9.05	0.045
CaCl ₂ × 2H ₂ O	1.91	0.013
<i>Density</i>	1.024	-
<i>Weight %</i>	3.42	-
<i>TDS</i>	33.39	-
<i>Ionic Strength</i>	-	0.657
<i>Ca²⁺/SO₄²⁻</i>	-	0.540
Ions	m [g/l]	m [mole/l] (molar)
HCO ₃ ⁻	0.12	0.002
Cl ⁻	18.62	0.525
SO ₄ ²⁻	2.31	0.0240
Mg ²⁺	1.08	0.045
Ca ²⁺	0.52	0.013
Na ⁺	10.35	0.450
K ⁺	0.39	0.010

Table A-2.3: Composition of fifty times diluted synthetic seawater, d₅₀SW.

Salt	m [g/l]	m [mole/l] (molar)
SSW	0.77	-
NaCl	0.468	-
Na ₂ SO ₄	0.068	-
NaHCO ₃	0.003	-
KCl	0.015	-
MgCl ₂	0.085	-
CaCl ₂ (dry)	0.029	-
MgCl ₂ × 6H ₂ O	0.18	0.001
CaCl ₂ × 2H ₂ O	0.04	-
<i>Density</i>	1.024	-
<i>Weight %</i>	0.07	-
<i>TDS</i>	0.668	-
<i>Ionic Strength</i>	-	0.013
<i>Ca²⁺/SO₄²⁻</i>	-	0.540
Ions	m [g/l]	mM [mmole/l] (mMolar)
HCO ₃ ⁻	2.5	0.040
Cl ⁻	372.3	10.503
SO ₄ ²⁻	46.1	0.480
Mg ²⁺	21.6	0.891
Ca ²⁺	10.4	0.259
Na ⁺	206.9	9.002
K ⁺	7.9	0.201
	667.8	-

Table A-2.4: Composition of Low Salinity Aluminum, LowSal Al, 10 mM.

Salt	m [g/l]	m [mole/l] (molar)
SSW	0.50	-
NaCl	0.50	0.009
AlCl ₃	1.333	0.010
<i>Density</i>	1.024	-
<i>Weight %</i>	0.19	-
<i>TDS</i>	1833	-
<i>Ionic Strength</i>	-	0.069
<i>Ca²⁺/SO₄⁻</i>	-	-
Ions	m [g/l]	mM [mmole/l] (mMolar)
Cl ⁻	1.37	38.6
Na ⁺	0.2	8.6
Al ³⁺	0.27	10.0
	1.83	-

Appendix 4: Cation and Anion Content

Table A-4.1: Cation Content, Calcium

Sample #	PV injected	Ca ²⁺ content [mMole/liter]
2	1.82	727.33535
3	4.37	725.86116
6	5.27	715.94342
8	8.35	723.36164
9	8.68	729.45214
10	9.33	668.92040
12	12.90	31.86055
14	15.94	21.99007
15	16.57	20.09535
16	17.07	16.65556
18	20.58	21.69239
19	21.40	23.08154
21	24.65	61.42949
23	25.20	40.16707
28	28.99	37.07221
31	30.06	35.01212

Table A-4.2: Anion Content, Sulphate.

Sample #	PV injected	SO₄²⁻ content [mMole/liter]
2	1.82	0.08873
3	4.37	0.06276
6	5.27	0.06060
8	8.35	0.06925
9	8.68	0.05843
10	9.33	0.03895
12	12.90	24.43499
14	15.94	24.58215
15	16.57	25.07773
16	17.07	25.27683
18	20.58	1.17728
19	21.40	0.94139
21	24.65	0.67087
23	25.20	0.88079
28	28.99	0.22507
31	30.06	0.22507